Nanoparticle heterogeneity: an emerging structural parameter influencing particle fate in biological media?

Jean-Michel Rabanel [a, ‡,*], Vahid Adibnia [b,*], Soudeh F. Tehrani [b,*], Steven Sanche [b], Patrice Hildgen [b], Xavier Banquy [b, ‡], Charles Ramassamy [a, ‡]

[a] *Centre INRS Institut Armand-Frappier, 531, boul. des Prairies, Laval, QC H7V 1B7 Canada*

[b] *Faculté de Pharmacie, Université de Montréal, C.P. 6128, Succursale Centre-ville, Montréal, Québec, H3C 3J7, Canada*

[‡] Corresponding authors: jean-michel.rabanel@iaf.inrs.ca; xavier.banquy@umontreal.ca; charles.ramassamy@iaf.inrs.ca

[*] These authors contribute equally

Table of content

Graphical Abstract

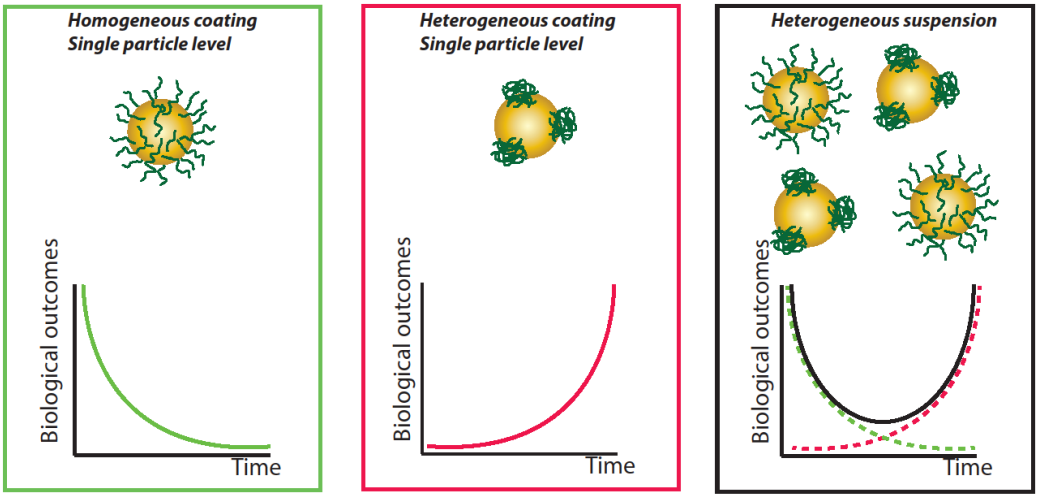

Abstract

Drug nanocarriers surface chemistry is often presumed to be uniform. For instance, the polymer surface-coverage-density and distribution of ligands on nanoparticles are described with averaged values obtained from quantification techniques on a particle population. However, these averaged values may conceal heterogeneities at different levels, either because of the presence of particle sub-populations or because of surface inhomogeneities, such as patchy surfaces on individual particles.

Characterization and quantification of chemical surface heterogeneities are tedious tasks, which are rather limited by currently available instruments and research protocols. However, existence of heterogeneities could contribute to some non-linear effects observed during nanoformulation optimization process, could contribute to problems related to nanocarrier production scale-up and could correlate with unexpected biological outcomes. On the other hand, these heterogeneities, while usually unintended and detrimental to nanocarrier performance, may, in some cases, be sought as adjustable properties that provide NPs with unique functionality.

In this review, results and processes related to these issues are compiled, and perspectives and possible analytical developments are discussed.

Key words: PEG, heterogeneity, nanoparticle, liposomes, ligand, ligand clustering, patchy nanoparticle, phase separation

Introduction

The accumulation of drug nanocarriers at pathological sites such as tumors and brain parenchyma, in spite of the "enhanced permeability and retention" (EPR) effect [1], intensive optimization of formulation and the addition of targeting ligand, is deceptive. Only a few percent of the injected dose is effectively accumulated at the targeted site [2-4], while 90 to 99% is distributed in non-targeted organs, potentially contributing to adverse effects. This issue is particularly critical for the delivery of active compounds to central nervous system as the blood brain barrier acts as a formidable obstacle to nanoparticles (NPs) entry. Different reasons have been suggested for the specifically low accumulation and retention of nanoparticle formulations, which critically affects therapeutic efficacy. Considering the complexity of the biological processes, our knowledge about the interaction between different tissues and the surface of nanoparticles is still incomplete, leading to an inaccurate predication of NPs fate *in vivo.* The limited diffusion of NPs in tissues and across biological barriers has been also underestimated [3]. Another set of explanations can be regrouped around the concept of particle heterogeneity. For example, key physicochemical properties such as size, shape, elastic modulus and surface chemistry have been shown to have differential effects on protein opsonization and particle distribution in healthy tissues and tumors, as well as on toxicity [5-8]. More recent studies have shown that size dispersity and surface chemistry heterogeneity can directly modulate NP distribution *in vivo* [9, 10]. These observations can be attributed to the extreme sensitivity of biological systems "to sense" specific surface architecture of foreign nano-objects at the molecular level, with an unmatched resolution [11].

Particle heterogeneity can be classified according to two organization levels: at the suspension level, i.e. subpopulation of particles within a same batch exhibiting different properties and chemistry; or at the nanoparticle level, i.e. non-homogenous distribution of physicochemical properties in the core or at the surface of a single particle (Figure 1). With suspension heterogeneity, different nanocarrier populations within the same batch behave differently in terms of the therapeutic efficacy. As a consequence, the effective dose of nanocarrier having the optimal characteristics will be over- or under-estimated. Additionally the effective dose of optimal nanocarrier will be also highly sensitive to batch to batch variability. Additionally, the NP sub-populations which are not effective may be detrimental, and could trigger toxicity or unwanted immune system reactions from the host. The single particle heterogeneity has also the potential to alter the specific interactions between the nanocarrier surface and proteins [12], or membrane [13, 14] *in vivo*, causing unexpected therapeutic outcomes.

Every day, new and more complex nanocarriers are being tested in research labs and clinical settings. The frequent use of responsive smart materials and bio-mimetic delivery strategies contributes to the constantly increasing complexity of the newly developed formulations. This also translates into complex synthesis, purification and formulation steps, which tremendously complicates their characterization and compliance with regulatory guidelines [15]. However, little concern is raised about the challenges from defects and heterogeneities of these complex nanostructures. Most fabrication processes do not allow rigorous control over homogeneity, because of complex and difficult to control physical mechanisms, such as phase separation, kinetic control of the assembly, mixing homogeneity and purification. The control of homogeneity at nanoscale is non-

trivial, and higher number of reaction/fabrication steps increases the probability of defect and inhomogeneity.

Certainly one of the most illustrative examples of how suspension heterogeneity affects biological outcomes is the impact of particle size dispersity. Small NPs (<150 nm) are reported to be more effective than large NPs in cancer therapeutic [16]. However, in several cases, it has been shown that relatively large NPs may serve as better drug carriers. For example, after studying different micelle batches with hydrodynamic diameters ranging from 22-300 nm (mean diameters determined by DLS), Wang *et al.* showed that the optimal size for blood circulation time and tumor accumulation was 100-160 nm [17]. However, larger micelles (100-160 nm) had poorer tumor penetration than the small ones (30 nm), highlighting the necessity for attentive size control [17].

Thus, nanoparticle batch size heterogeneity can also significantly influence biodistribution and targeting. The role of particle size on *in vivo* efficacy has been recently discussed [10, 18]. In the case of PRINT® NPs ("Particle Replication In Non-wetting Templates"), particle size appeared to be the main factor in NP tumor accumulation *in vivo* rather than the specific ligand density or particle shape [18]. Another example is Poly(lactic-co-glycolic) NPs (PLGA NPs) produced by emulsion-solvent evaporation technique, which notoriously results in a heterogeneous size distribution. In an experimental study, a PLGA NP batch carrying a plasmid encoding luciferase protein was fractionated over a 100 nm pore-size filter, resulting two NP fractions having a mean diameter of 70 and 200 nm. It was shown that luciferase transfection efficiency was 27-fold higher with smaller NPs (mean diameter 70 nm) compared to larger NPs (mean diameter 200 nm). This result was obtained despite surface charges, DNA release and cell

entry were found near identical for the two NP fraction of the same batch [19]. Considering these examples, a polydisperse NP suspension may induce different biological outcomes with respect to its size distribution.

Although surface heterogeneity could be an issue in terms of the particle batch performance, in some recent studies the NP's surface was intentionally manipulated to induce heterogeneities [20, 21]. The aim is to take advantage of these heterogeneities to modify NP's interactions with biological media, modify drug release profile or promote the formation of ordered particle-based superstructures.

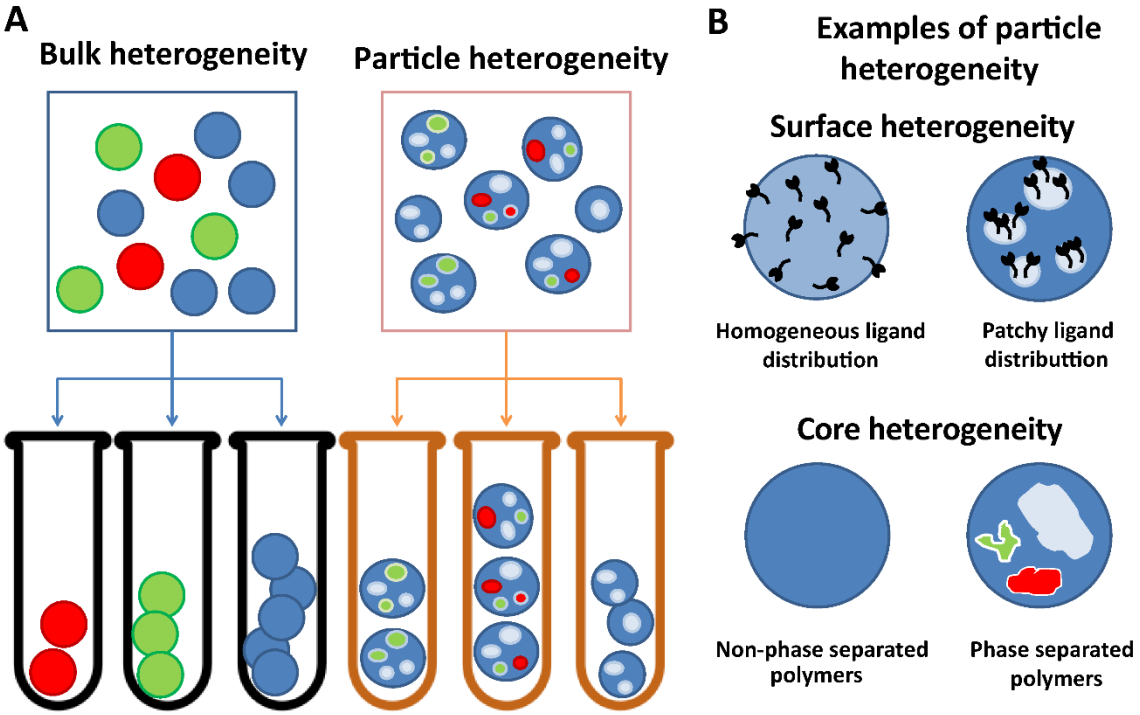

Figure 1 ***(A)*** *Schematic representation of the heterogeneity at the suspension level (left) and at the single particle level (right). In both cases averaged value can be obtained for each physicochemical property. (B) Some examples of NP surface heterogeneities influencing global biological performance and particles fate; at the nanoparticle suspension or the single particle level: (top right) homogenous ligand density; (top left) surface ligand clustering; (bottom right) homogenous material surface; (bottom left) material phase separation on surface produces domains of different composition.*

The heterogeneity of physicochemical properties within a nanocarriers population is an emerging issue and concern. In this review, recent results regarding the chemical heterogeneity are discussed (see Figure 2 for selected examples of particle heterogeneity imaging). Size heterogeneity will be discussed only with the perspective of its role in the variation of chemical composition and topology, since size fractionation could be related to distinct chemical compositions. The focus will be on chemical heterogeneity: core composition, hydrophilic corona layer heterogeneity and ligand density heterogeneities. The discussion of this review will focus on the methods to highlight this heterogeneity, some consequences on *in vivo* performances, the potential source of this heterogeneity and how to minimize or in some cases optimize it.

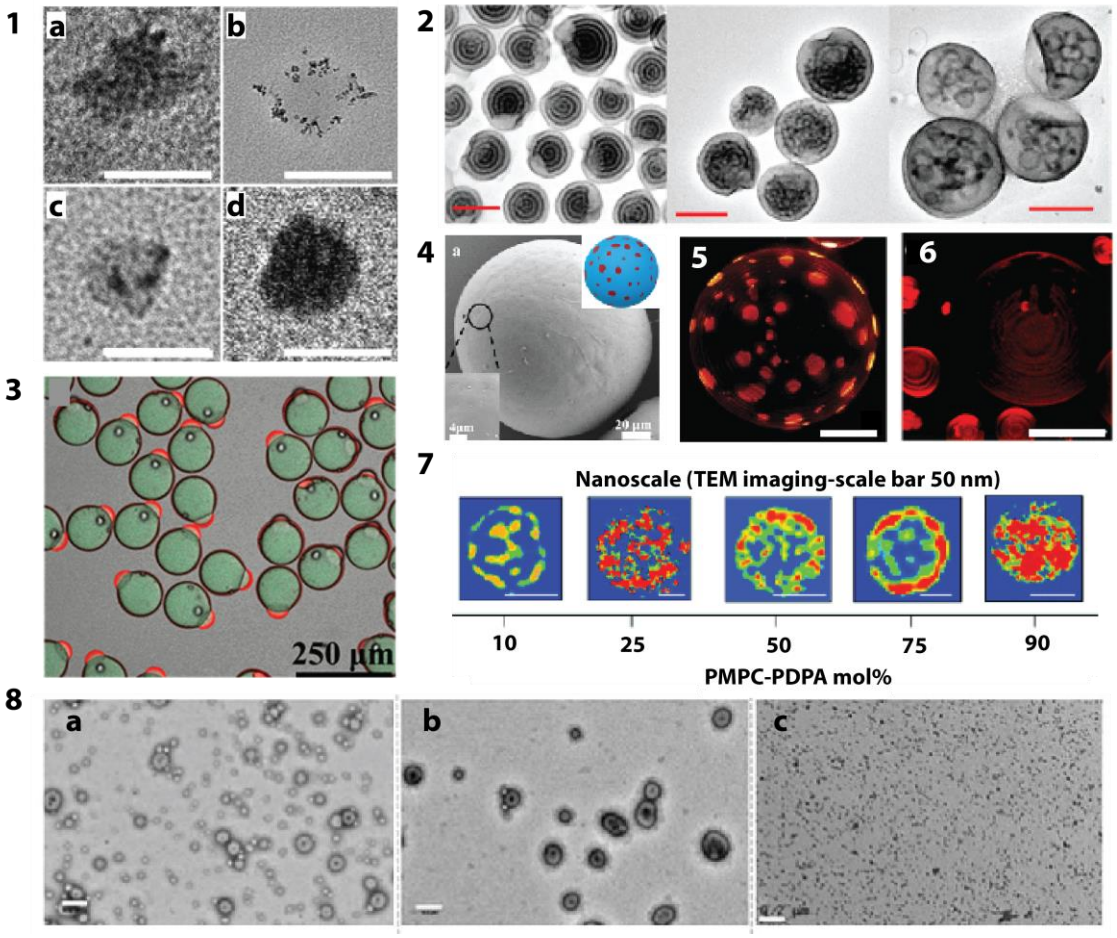

Figure 2 Examples of nanoparticle heterogeneity: ***(1)*** *TEM images of representative formulations showing the clusters of ligand on the micelle surface. Scale bars show100 nm. Reprinted with permission from Poon et al.* [22] *;* ***(2)*** *TEM images of internal structure heterogeneity of PS/PI block polymer particles. Scale bars are 200 nm. Dark gray regions are PI domains stained with OsO4. Adapted with permission from Grundy et al.*[23]*;* ***(3)*** *Confocal optical microscopy of phase separation in PCL/PLGA microcapsule shell under slight osmotic pressure. The shell fluorescence is from Nile red (in PCL-rich phase), reprinted from* [24] *with permission;* ***(4)*** *Intermediate state of phase separation in the microcapsule shell (PCL and PLGA): structure of a patchy microcapsule. SEM image Reprinted with permission from reference.*[24]*;* ***(5)*** *Imaging an oscillatory phase separation. Z-stack projections of height-resolved fluorescence images of a giant unilamellar vesicle consisting of POPC:SM:Ch (1:1:1) labeled with 0.5% Rhodamine-DPPE, Scale bar shows 5 µm. Reprinted from* [25] *with permission;* ***(6)*** *Confocal microscopy image of hybrid lipid/polymer giant unilamellar vesicles (HLP-GUV) with irregular, star-shaped DPPC-rich domains in PBdPEO:DPPC (6 : 4) GUVs cooled to room temperature; Scale bar shows 10 mm. Reprinted with permission from Nam et al.* [26]*,* ***(7)*** *Fast Fourier Transform filtered TEM images obtained for selectively stained hybrid polymersomes prepared at different binary compositions showing the nanoscale*

*morphology, reprinted from LoPresti et al.[27]; **(8)** Illustration of size heterogeneity: TEM micrographs of the polymersomes solution (a) before AF4 separation; (b) after separation and (c) the separated micelle solution. Scale bars show 200 nm. Reprinted from Robertson et al. [28] with permission.*

1. Particle suspension heterogeneity

When heterogeneity is found at the suspension level, discrete particles subpopulation with distinct physicochemical properties and chemical composition can be identified within the suspension. Although this subject has not been studied extensively, some studies have reported subpopulation heterogeneity based on particle suspension fractionation. Particle fractionation has been mainly based on the size or the density of NPs essentially because the available techniques mainly operate based on particle mass or volume differences. As developed below, strong correlations between particle size and chemical composition were often described. Note that the size dispersity is not discussed in this review as a heterogeneity on its own. However, it is one of the important sources of creating surface or chemical heterogeneity in NP suspensions. Therefore, we discuss the relation between the size dispersity and chemical/surface heterogeneities, and the subsequent effect of such heterogeneities on the NP performance.

1.1. Effect of particle size on NP chemical composition

Recent reports have highlighted higher-than-expected variations in nanocarrier chemical composition correlated to their size polydispersity with important consequences on the performance. The influence of size polydispersity on the chemical composition and active delivery properties of lipid NPs encapsulating *si*RNA have been recently investigated [29]. Two similar lipid NP batches with similar bulk properties (chemical composition, hydrodynamic diameter, surface charge, and encapsulation levels) were

tested. The lipid NPs were fractionated on a size exclusion chromatography (SEC) column and fractions were analyzed for the chemical composition, lipid/encapsulated siRNA ratio and *in vitro* efficacy of gene silencing activity of *si*RNA. While one batch was found monodisperse (a uniform lipid composition across fractions), the second one showed a significant dispersity for all the parameters tested. *In vitro* gene silencing activity of the bulk batches and SEC fractions was evaluated. The two NPs batches without fractionation displayed overlapping dose-response curve. In contrast, fractions of the two batches showed significant differences for their *in vitro* activity, highlighting the importance of heterogeneity assessments [29].

In the case of polymeric NPs, the polymer composition and *Mw* can vary with NP size as demonstrated by Pirok *et al*. The authors developed a two-dimensional liquid chromatography (LC/LC) system, which combines hydrodynamic chromatography (HC) and SEC. The HC was used to fractionate a mixture of polystyrene and polyacrylate (PS/PACR) polymeric NPs based on their size, and SEC analyzed polymers composition of each NP fraction [30]. PS and PACR NPs were effectively separated in different fractions, but the technique showed a lack of resolution to separate PACR NPs of different size. The subsequent polymer SEC analyses gave insights on the polymer *Mw* and *Mw* distribution in the different NP fractions. Larger particles generally were composed of larger polymer chains, while *Mw* distribution was found to be modulated according to particle size [30]. The significance of these differences in polymer composition on different biological response remains to be established.

Preparation of NPs is often associated with the use of surfactant to control the size and stability of the resulting suspension. The amount of surfactant on particle surface

influences several surface properties. It has been shown that the particle size influences the amount of surfactant poly(vinyl alcohol) (PVA) adsorbed on PLGA nanoparticles [9]. Biological outcomes, such as cellular uptake and distribution for those particles could be explained not only in terms of size differences but also in terms of surface chemical composition differences [9, 31].

Surfactants have been also used as NP surface modifiers. For instance, Poloxamine 908 and Polysorbate 80 physioadsorbed on NPs were shown to induce a change in blood circulation time and organ biodistribution when a concentration threshold was reached [32]. These changes has been attributed to selective adsorption of plasma proteins on the NPs surface, enabling some sort of tissues targeting [33]. The existence of coating heterogeneity and its influence on NPs fate had not been investigated, even though the unstable nature of physioadsorbed coating *in vivo* can make it prone to shedding.

1.2. Effect of particle size on drug loading

For drug nanocarriers, bulk chemical composition heterogeneity can be the result of differential drug encapsulation in different particle sub-population. The relationship between particle size, drug loading (DL) and encapsulation efficiency (EE) had been previously addressed for particle suspensions with distinct size distributions. For protein-loaded microspheres which were size-fractionated by centrifugation, the loading efficiency was similarly found to depend on the microparticles size [34]. Gefitinib content in the collected polymeric microspheres was found to vary at least 3 times between the smaller MPs (<20 μm) and the larger ones (>100μm) [35]. This phenomenon has not been shown yet for NPs (size <1μm) but it could be expected according to this study.

1.3. Surface charges heterogeneity in a particle suspension

Evidence of chemical heterogeneity in particle suspension has also been demonstrated from diffusive measurements in complex matrices. NP suspension, prepared by polyelectrolyte assembly with near neutral surface charge, were shown to contain NP sub-populations with higher diffusion coefficient in mucus than the average NP population [36]. The difference in the diffusion coefficient was attributed to heterogeneity of surface charge. The authors explained that the process of self-assembly of polyelectrolyte polymers into NPs lead to surface charges that are not uniformly distributed. The result was surface domains with different charges, leading to different interactions with the mucin network [36]. This hypothesis is supported by results showing that the spatial organization and charge distribution composition on peptide, even with similar overall charge, can modulate their diffusion in a mucin gel [37].

1.4. Nanoparticle corona heterogeneity in a suspension

The surface of nanocarriers is usually constituted by a hydrophilic polymer corona, which plays a major role in colloidal stability, anti-fouling, pharmacokinetic and biodistribution. Polyethylene glycol (PEG) is by far the most used polymer for this purpose [38]. Therefore, the discussions in this section are mainly about this polymer. However, most of the principles discussed below can be applicable to other surface-tethered polymers.

1.4.1. PEG particle surface coverage

The antifouling efficacy of a PEG layer is related to its surface density, which is often characterized by a surface-density average value for a NP population [38]. PEG chain could

be in either a mushroom conformation or brush conformation depending on the coverage density and the length of PEG chains [39, 40]. PEG coverage-density heterogeneity may appears as (1) heterogeneity in the NP suspension when a sub-population of NPs has sub-optimal PEG coverage, (2) heterogeneity on the surface of individual nanocarriers, i.e. "bald spots" or low density zone due to fluctuation of PEG coverage, or (3) heterogeneity in corona thickness arising from the *Mw* dispersity of the surface-tethered polymers (Figure 3).

The variability of surface polymer density within the NP suspension has been shown to affect biodistribution of PEGylated NPs and liposomes *in vivo* [41, 42]. The presence of subpopulations with lower PEG coverage density also influences the overall therapeutic efficacy of the encapsulated drug. In addition, it can affect the NP diffusion in biological media [43] and ligand targeting efficacy [44, 45].

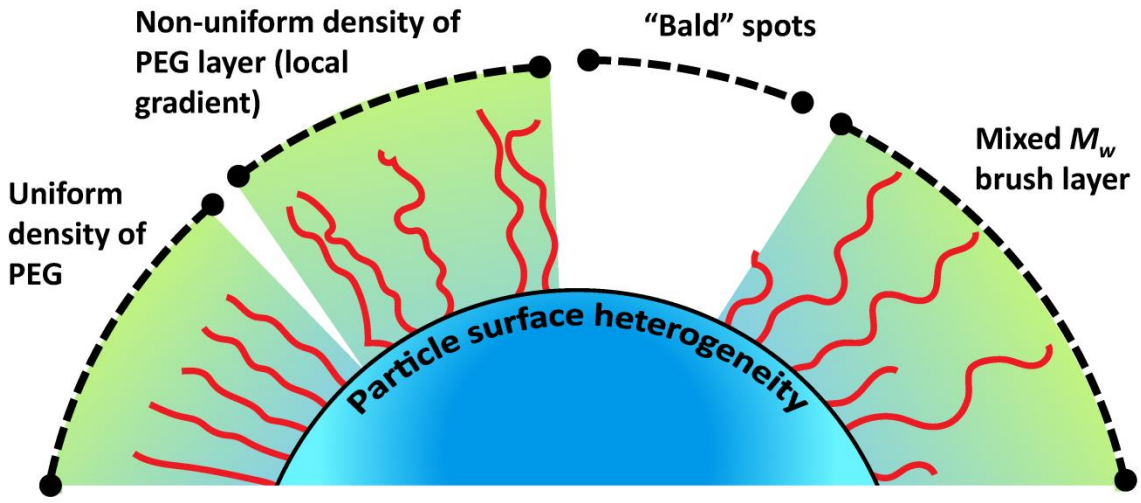

Figure 3. PEG surface layer heterogeneities, from left to right: uniform density on the surface, variable PEG surface densities (PEG/nm^2); "bald spots", mixed molecular weight PEG brushes.

1.4.2. PEG surface heterogeneity and subpopulations

Surface composition is challenging to characterize particularly homogeneity of surface coverage [11]. The averaged PEG chain surface density (PEG chain/nm^2) is calculated from NP ensemble averaged measurements [38]. Although not extensively studied, the PEG heterogeneity in PEGylated polymeric particle populations has been documented by Moghimi and coworkers [46, 47]. Using hydrophobic interactions chromatography (HIC), the authors were able to characterize the heterogeneity of a population of polystyrene microspheres (MPs) after PEG grafting. Since the level of surface hydrophobicity relates to the PEG grafting density, suspensions of MPs, with different surface hydrophobicities, were found to behave differently regarding macrophage uptake, protein binding and circulation time in blood [47].

Besides surface density heterogeneity, the polymers corona thickness could be modulated by the molecular weight distribution. When PEG chain length is increased, an increase in the distance between tethered polymer chains is observed resulting in a decrease in coverage density due to the excluded volume effect. A lower coverage density decreases the antifouling efficacy of the PEG layer [48]. To maintain surface anti-fouling efficacy, several studies have proposed mixed/heterogeneous PEG layers. Indeed, it has been shown, on flat surfaces modified with a PEG 5kD, that the addition of a short "underbrush" layer of 2kD PEG leads to a decrease in non-specific protein absorption [49-51]. Studies on liposomes demonstrated the benefit of this approach on the circulation time [52, 53]. Colloidal stability of gold NPs has been improved using mixed-molecular-weights PEG layer as well [54]. Likewise, “hetero-brush” PEG surface (with 2kD “underbrush” and 5 to 20kD PEG chains “over brush”) on peptide nanospheres show greater proteins

resistance and serum stability than “homo-brush” PEG surface with 2kD or 5kD chains [55].

The quantification of PEG chains with different *Mw* values on the same NPs is a challenging task that is yet to be overcome. This is important to ensure that the optimal ratio between PEG chain lengths is maintained through the preparation process, and that the surface is covered by a uniform mixing of the different chain lengths to avoid possible phase separation phenomenon [48].

1.5. Ligand surface distribution in suspension

Heterogeneity in ligand-modified surfaces may appear either with a variable number of ligand per nanocarriers or with a non-uniform spreading or clustering of ligands on the surface of a single particle (Figure 1B). The latter will be addressed in section 2. It is well established that ligands multivalency improves the affinity of ligand-modified carriers toward targeted cells [56], cell internalization [57] and drug encapsulating efficiency [58]. Quantitative determination of ligand density, although an indispensable step toward optimization, is suffering from lack of accurate techniques to quantify ligand number on individual particles. The quantification is often performed based on the knowledge of particle concentration, particle total surface area and core diameter[38, 59].

Numerous studies tried to address the question of the optimal ligand number and density to achieve high specific endocytosis and/or tumor accumulation [18, 60, 61]. However, these studies rarely took the heterogeneity of ligand number per particle (ligand-to-nanoparticle ratio) into account. They often exclusively used the average values for this characterization. The average value, however, does not recognize the distribution of ligand number and its eventual dependence over other physicochemical parameters such

as particle size. Another concern is the sensitivity of the ligand grafting reaction to surface heterogeneity such as surface roughness which could modulate coupling reaction rate and reaction kinetics [62].

The number of ligand present on nanocarriers can vary, even on narrowly-dispersed structures such as Polyamidoamine (PAMAM) dendrimers [63]. The most disturbing observation is that the most abundant species are, in many cases, the unmodified dendrimers without grafted ligand [62]. Another issue is that the average value could be very different from the median or mode values, as shown in Figure 4, pointing out that the information provided by an average value alone is not always as reliable as it is perceived [63].

To the best of our knowledge no other similar analysis has been conducted for ligand modified nanoparticle or liposomes, even though similar issues might occur. Indeed, separating NPs according to their ligand number density is technically challenging, and so far the above example with dendrimers is the only one reported.

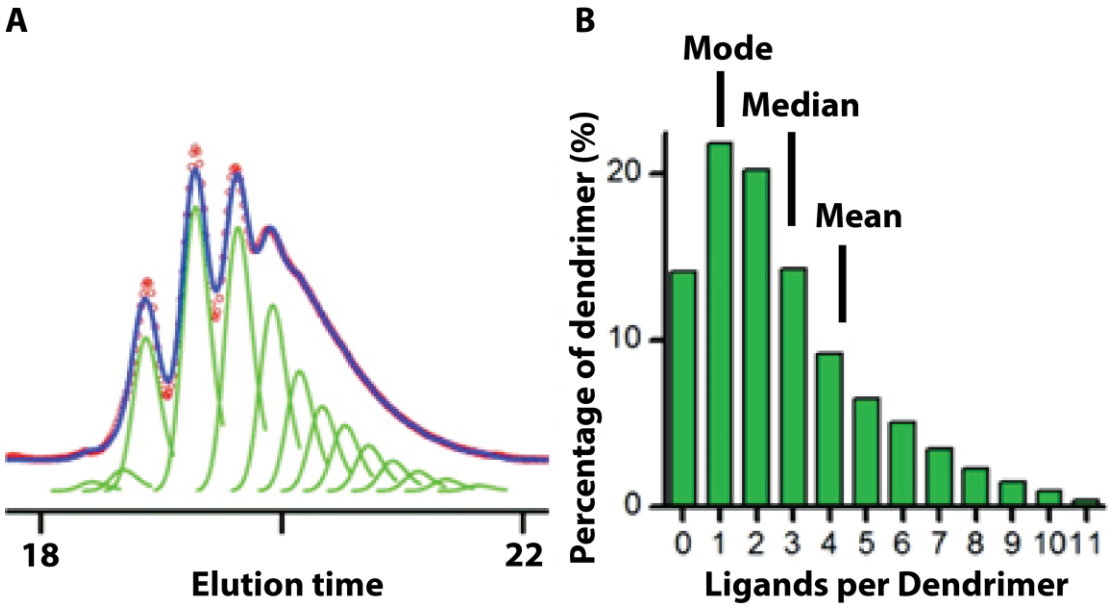

Figure 4 (A) Peak fitting method quantifies the distribution of dendrimer−ligand species resolved in the HPLC elution traces. (B) Dendrimer−ligand distributions. Adapted from reference [63] with permission.

2. Single particle heterogeneity

2.1. Hydrophilic corona heterogeneity at the single particle level

As mentioned earlier, another type of PEG coverage-density heterogeneity can be deleterious to nanocarriers performance: heterogeneity on the surface of individual nanocarrier, *e.g.,* "bald spots" or low density regions due to fluctuation of PEG brush coverage. Low PEG surface densities are prone to protein adsorption [64]. Thus, these surface heterogeneities can lead to accelerated opsonisation and mononuclear phagocytic system (MPS) uptake and elimination[6].

It has been reported that gelatin NPs observed by atomic force microscopy (AFM) topographic imaging show rougher surface when modified with PEG. This roughness suggests that PEG chains are not distributed homogeneously on the surface [65]. Differences in stiffness between PLA and PEG have been used to visualize surface heterogeneity caused by PEG/PLA phase separation at the surface of NPs [66, 67]. Other indirect evidences of PEG surface heterogeneity have been provided by XPS analyses. In PEG-*g*-PLA NPs, shift in the carbon peaks positions suggests existence of areas with different charge accumulation on the NP surface, which in turn supports the presence of PEG enriched regions [66].

At this point, there is a clear lack of accessible and direct techniques to allow surface PEG quantification and characterization at the individual particle level that hinders complete understanding of the possible role of heterogeneity on nanocarriers performance and further process optimizations.

Similarly, uneven distribution of PEG chains on the surface of liposomes has been reported due to phase separations of PEG-lipids [68, 69]. It has been suggested that longer PEG chains interact via van der Waals forces and interchain hydrogen bonding, causing chain entanglement that leads to enriched PEG domains [68]. PEGylated lipid also influences hydrocarbon chain packing, favoring a temperature dependent phase separation [69]. Potentially, it cannot be overlooked that a similar effect could happen when forming solid NPs, nucleic acid-PEGylated polymer assembly or during PEG grafting. These points are discussed further in the origin of heterogeneity section.

Spatial organization and assembly of lipids were at the origin of heterogeneity in liposome suspension. Heterogeneity in liposome surface organization was found responsible for the existence of two liposome populations having distinct stability properties and affinity for surfaces. The heterogeneity was attributed to differences in the number of surface hydrophobic active sites which leads to spontaneous leakage of content and increase in the affinity for hydrophobic surfaces [70].

It is well known that different curvature radius of spherical nanocarriers affect PEG chains layer packing [6]. In the case of gold non-spherical particle (AuNPs), coverage heterogeneity could arise from faces, corners and edges which could either induce a local non-optimal packing of the PEG layer, or local variation of the grafting efficiency [71].

2.2. Ligand distribution on a single particle

As discussed earlier, ligand multivalency plays a major role in targeted system affinity. The interplay between ligand and surface chemistry is another important parameter because it could influence targeting efficacy. For example surface PEGylation may decrease ligand affinity [72 73]. Xu *et al.* have shown that nanodomains located on a

lipoplex particles carrying plasmid DNA can affect transfection efficacy. The authors demonstrated that targeting was improved when specific ligands (folate) were located in cholesterol-rich lipid domains on the NPs surface. PEGylation of lipoplexes usually results in a decrease of plasmid DNA transfection efficacy. PEGylation of lipoplexes with DSPE-cholesterol conjugate results in PEG chains to be located mainly in the cholesterol-rich domains. In this case, the transfection efficacy was not affected [74]. The question, whether this effect was mediated by the change in physical properties of the carrier surface, such as ligand clustering, remains unanswered.

In another study, clustered or patchy presentation of ligands has also been shown to influence the targeting efficacy [22]. Clustering of ligands bound to the polymer end-groups was observed in a micellar system constituted by dendritic polymers. Clustered ligand presentation increases the efficacy of NPs due to their enhanced uptake, which is resulted from the higher avidity and longer residence time in cell membrane [22]. Tumor targeting of polymer-based nanovesicles was improved both *in vitro* and *in vivo* using vesicles made of lipid/polymer blends [75]. The authors attributed this improvement to the "dilution" effect of the PEG brush density at vesicles surfaces when lipid/polymer composition was modulated. PEG brush can presumably have a negative effect on ligand-receptor recognition under certain conditions. On the other hand, Dao *et al.* showed recently by Fluorescence Resonance Energy Transfer (FRET) analysis and Small-Angle Neutron Scattering (SANS), that phase separation between polymer and lipid occurs in hybrid polymer-lipid vesicles, which can lead to the formation of nanodomains that impacts the biological activity of NPs [76]. Surface clustering of the folate ligand enhances cellular internalisation of NPs compared to a dispersed more homogenous distribution [77].

3. Engineered heterogeneity

Although heterogeneity is generally perceived as a negative factor in nanomaterial performance, in some cases, such as for ligand clustering discussed above, it has been studied as another adjustable surface property. Indeed, some reports have shown that NPs with patchy polymeric surfaces favor cell internalization, modulate drug release and drive particle auto-assembly. In these cases, the surface has engineered heterogeneity.

3.1. Chemically anisotropic nanoparticles and superstructures

Engineered NP heterogeneity results in anisotropic particles that can be categorized as Janus, multi-compartment and patchy particles as illustrated in Figure 5. Patchy particles have domains of varying properties on their corona, whereas in Janus NPs, two distinct phases are separated either in the corona or in the core.

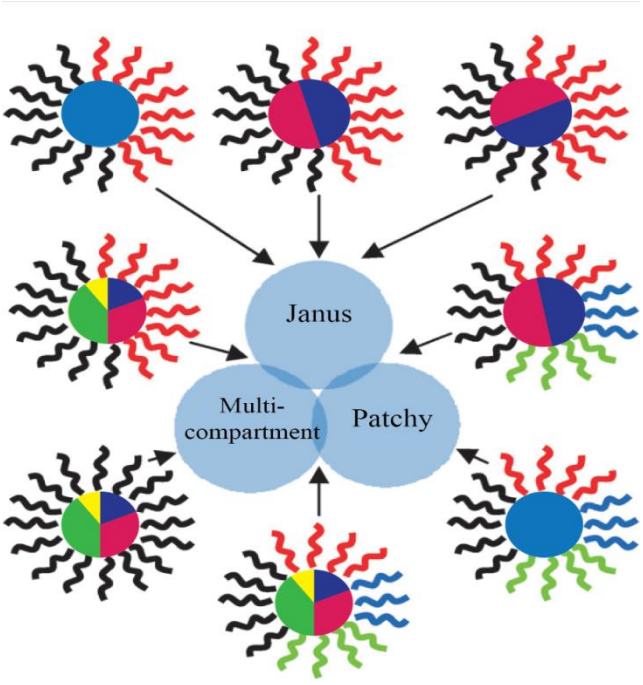

Figure 5. Schematic representation of Janus, patchy and multi-compartment NPs. The different possible combinations of these structures are also depicted. Adapted from Du and O'Reilly [20] with permission.

Multi-compartment particles are similar to patchy particles with the difference that the multiple phase-separated domains are present in the core of the NP rather than in the corona. Combinations of these three types of inhomogeneity produce a large spectrum of complex anisotropic particle structures. In this section we review some of the most recent designs of these novel classes of NPs. For more information on fabrication and assembly of these NPs refer to Pawar and Kretzschmar (2010) [78], Du and O'Reilly (2011) [20], Liu *et al.* (2015) [79], Ravaine and Duguet (2017) [21].

Mixtures of polymer and lipids have been proposed for membrane and lipo-polymersomes preparation. The mixing of these two types of materials creates new hybrid vesicles for drug delivery if the preparation conditions are well adjusted (temperature, ratio and speed). For the preparation of hybrid lipo-polymersomes, Nam *et al*. used phase separation upon mixing and demixing of lipids and diblock polymer to generate surface domains. The resulting surfaces have varying domains in hybrid lipo-polymersomes [26].

As evident in the numerous reviews published on this subject, the production of patchy particles is now efficiently done. However, non-random patterning of NPs, except for Janus surface patterning, is not as convenient. In an interesting study aimed at controlling surface patterns, Choueiri *et al.* in 2016 used thermodynamically driven segregation of polymer ligands, from a uniform polymer brush into surface pinned micelles, by changing the solvent quality [80]. This methodology appeared to be effective in controlling

the dimensions of the patches, their spatial distribution and their surface density. Although the initial mechanism results in reversible formation of the patches, their shape and configuration can be frozen using photo-crosslinking. The formation and shape of these particles are illustrated in Figure 6. In a similar study, Ye *et al.* experimentally and theoretically showed that the number of patches is inversely proportional to the concentration of patch-forming blocks [81].

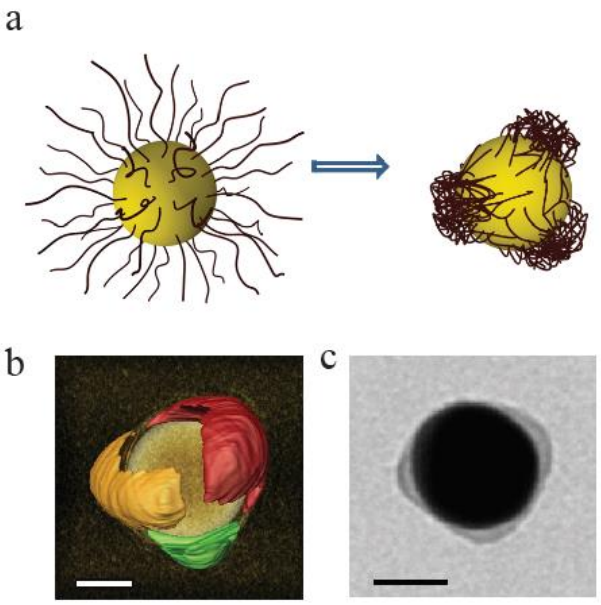

Figure 6. (a) Schematic representation of the solvent-mediated formation of the surface patches on NP surface. (b) Electron tomography reconstruction image of a 60 nm nanoparticle with three patches of polystyrene with a grafting density of 0.02 chains per nm^2. TEM image of a gold NP carrying photocrosslinked thiol-terminated polystyrene-co-polyisoprene patches. Scale bars in b and c are 20 nm. Adapted from Choueiri *et al.* (2016) [80] with permission.

Multicompartment micelles can be produced, using linear ABC triblock terpolymer via a step-wise reduction of the degree of conformational freedom and dynamics [82]. In the first step, the triblock terpolymer self-assembles into a core-shell geometry when exposed to a non-solvent for the B block. This step leaves A and C blocks in the corona. During the

next step, exposure to a non-solvent for the A block triggers the collapse of block A, leading to higher-level assembly of the subunits into the final superstructure as shown in Figure 7.

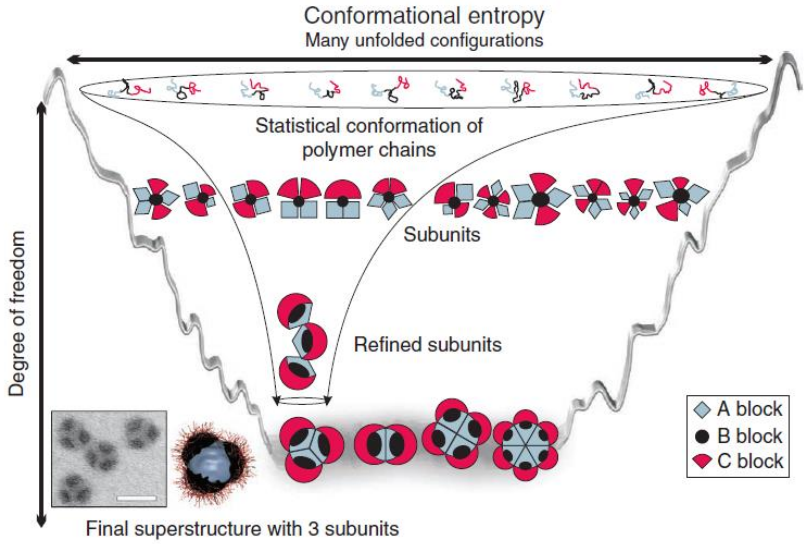

Figure 7. Mechanism of the directed hierarchical self-assembly of triblock terpolymers in solutions. The scale bar is 50 nm. Reprint from Groschel *et al*. (2012) [82] with permission.

Under suitable conditions, the colloidal polymerization of these self-assembled NPs can be used to produce segmented superstructures [82]. Similar multicompartment micelles were used to produce anisotropic colloidal polymers with segmented structure [83]. An interesting sequel of this work was recently published by Lobling *et al.* in 2016 where these NPs (with C corona and A/B cores) were used to produce nanostructures with controlled patch morphology (see Figure 8) [84]. The ratio of the blocks length N_C/N_A was found to control the transition from micelle geometry to sphere, cylinder, sheets and vesicles, while length of the B block, N_B, controls the patch morphology from spherical

to cylindrical, bicontinious and lamellar. The result is a large library of patchy-multicompartment nanostructures as shown in Figure 8.

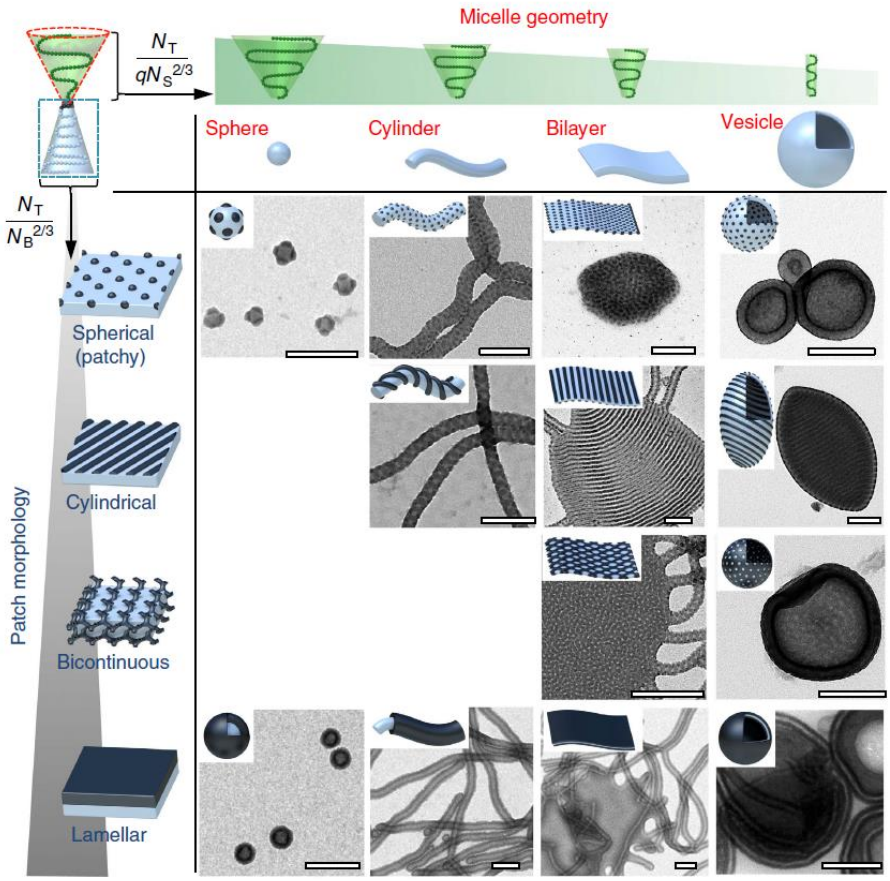

Figure 8. Sub-classifying patchy-multi-compartment nanostructures based on micelle geometry and patch morphology. The scale bars are 200 nm. Reprinted from Lobling *et al.* (2016) [84] with permission.

Massignani *et al*. reported the fabrication of novel polymersomes using poly(2-(methacryloyloxy) ethylphosphorylcholine)-co-poly(2-(diisopropylamino)ethylmethacrylate) (PMPC–PDPA) and poly(ethylene glycol)-co-poly(2-(diisopropylamino)ethyl methacrylate) (PEG–PDPA) diblock copolymers comprising an hydrophilic block (PMPC, PEG) and a pH-sensitive block (PDPA). When the copolymers are mixed in different ratios, they result in polymersomes, having surface

phase separation as evidenced by staining and visualization by TEM. The patchy PMPC/PEG surfaces show differences in cell internalization rates, relative to the surface polymer [85].

3.2. Applications of the engineered heterogeneity

The increasing attention towards the production of chemically anisotropic particles is fueled by the numerous potential applications of this novel class of materials. Self-assembly of polymers into desired nano- and micro-patterned structures can be employed in biomedical, electronic and energy applications. Perhaps the most intriguing application is the formation of self-propelled nano/micro particles which can be used for efficient micro/nano mixing. In this section, while focusing on biomedical applications, we review some of the recent literature on chemically anisotropic particles.

Verma *et al.* showed that 6 nm nanoparticles, coated with a shell of hydrophobic and anionic ligands regularly arranged into ribbon-like domains of alternating composition penetrate cell membranes without evidence of membrane disruption. On the other hand, particles with identical hydrophobic content but without structural order in the ligand shell do not penetrate cell membranes. The authors concluded that structural organization of surface chemical groups plays a key role in regulating cell-membrane penetration [13].

The self-propelling property of Janus particles has been studied experimentally and theoretically by Howse *et al.* By coating half of the surface of polystyrene MPs with platinum, the authors showed that at short times, the particles trajectory was predominantly ballistic with velocities in the μm/s range, while at longer times the motion was random. This example interestingly illustrates how Janus structures (or

potentially other chemically anisotropic particles) can be employed for designing chemical locomotive systems [86].

With the ultimate objective of improving the delivery of macromolecular therapeutics to the cellular cytoplasm, Imam *et al.* (2017) studied the effect of lipid membrane phase separation on membrane fusion. They demonstrated that phase separated vesicles transferred their content into the cellular cytoplasm four times more efficiently than homogeneous vesicles [87]. Heterogeneous surfaces could potentially be used as tools to understand cellular functions [88], modify NP biodistribution [89] and increase antifouling properties [90, 91]. Many more applications of chemically anisotropic particles in drug delivery was reviewed by Tran *et al.* in 2014 [92].

4. Analytical methods to characterize heterogeneity: recent developments

Few methodologies are available to assess heterogeneity since the development of proper analytic tools for this purpose is still at its infancy. The techniques may vary depending on whether heterogeneity at the suspension level or at the single particle level is characterized.

4.1. Detection of heterogeneity in particle suspension

4.1.1. Fractionation of particle suspensions

Several studies have reported the use of fractionation of particle suspension by size, density or surface properties to assess their chemical compositions, efficacy and fate *in vivo*. Several fractionation methods have been reported: fractionation based on particle size with Size Exclusion Chromatography (SEC) [63], Asymmetric flow field flow fractionation (AF4) [93 94, 95] or centrifugation [96]. Centrifugation fractionation can be based

on particle density with isopycnic centrifugation [97, 98], or sedimentation velocity analytical ultracentrifugation [99-101]. Least common is fractionation based on affinity chromatography since separation cannot be achieved for nanoscale objects [47].

Heterogeneity in size and shape has been also highlighted in studies on NPs purification since NP subpopulation could be detected during purification procedures [28, 102]. Fractionations based on other properties than size and density, such as ligand number, are rarely reported except for the study by Mullen *et al.* discussed above in section 1.5 [63].

Following fractionation, NP subpopulations can be analyzed using conventional techniques to determine for instance, chemical composition, ligand numbers or other physicochemical parameters. These results could be confronted to average values obtained from the entire NP population to draw conclusions on NP batch heterogeneity.

4.1.2. Direct analysis of nanoparticle suspensions

Techniques that rely on a direct analysis of the NPs are useful for identifying heterogeneities within a suspension. For example, observation of thousands of liposomes by confocal microscopy along with fluorescent signal processing, can identify lipid composition heterogeneity between liposomes of the same batch [103]. The technical and practical aspects of individual liposome visualization by confocal microscopy as proposed by Larsen *et al.* [103] is more detailed in section 4.2. The lipid composition was reported to vary significantly (ten-fold) between liposomes, which can impart drastic effects on their physicochemical properties. Such composition heterogeneity could not be identified using conventional techniques that rely on averaged properties over the entire particle population. Despite the valuable information obtained using such direct observation, high throughput screening of particles is often impossible. Therefore, it is

important to assess the possibility of using other characterization techniques for detecting heterogeneities.

Electrophoretic methods (EM) are able to screen small NPs and identify size and charge heterogeneity based on their electrophoretic mobility. The mobility depends on NP charge, size, shape and surface functionalization. This technique can be divided in two main categories: gel-based and gel-free separation.

Doane *et al.* applied the gel electrophoresis (GE) method to quantify the electrophoretic mobility of PEGylated gold NPs (Au NPs) according to the PEG-ligand molecular weight and hydrodynamic radius. Since different PEG molecular weights produce different gel migration patterns, this technique was applied to characterize and separate NPs according to their PEG-ligand molecular weight difference[104]. A similar approach was applied by Daou *et al* to separate PEGylated quantum dots according to the PEG-ligand molecular weight [105]. Gel electrophoresis has also been applied to separate Au NPs modified by monofunctional methoxy-PEG according to the PEG-ligand surface density [106]. However, GE is rather limited by the size range, typically only NPs smaller than 25 nm can be resolved due to the gel pore sizes.

Capillary electrophoresis is extensively used to study several physicochemical parameters of a population of nanoparticles and nanoparticle-biomolecule conjugates [107-109]. By coupling capillary electrophoresis with laser-induced fluorescence detection, Duffy *et al.* were able to detected individual sulfated polystyrene particles loaded with a fluorescent dye. Using this approach, chemical heterogeneity, surface interactions, double-layer ion distribution, size and ζ-potential can be studied at the single particle level, and separation based on these parameters can be undertaken [110]. Rezenom *et al.*

reported that a small number of individual particles can be characterized, and the detection efficiency in this technique ranged from 38 to 57% for different particle sizes [111].

Polystyrene particles (PS) functionalized by amino, carboxylate, and sulfate were separated and characterized by capillary electrophoresis-UV according to their difference in surface charge [108]. The separation was achieved for significant surface charge difference between functionalized PS particles (more than 20-30 mV difference in surface potential and charge inversion); whereas, charge difference inside the same batch of NPs is usually less significant (SD about +/-10 mV). Therefore, optimization is necessary before this technique could be used to resolve heterogeneity inside a suspension of NPs. An important point is that samples in capillary electrophoresis are in an electrolyte solution. Therefore, NPs stability in solution must be carefully monitored [109, 112]. Other critical points to be considered are the improvement of resolution, reproducibility and current lack of reference nanomaterials to be used as standard in analytic methods [109].

Industrial applications of colloidal particles, such as inks and paints, usually require samples concentration far above the concentration and turbidity limits that the light scattering techniques can operate in. In addition, in large scale production of nanoparticles it is preferred to measure the properties (especially NP size and ζ-potential) in real time so that a control system can respond and eliminate any defected sub-populations, thereby decreasing the heterogeneity in the final product. Electroacoustic spectroscopy, a technique that operates based on electrokinetic phenomena at megahertz frequencies, is an ideal characterization method for concentrated nano- and micro-particle

suspensions and industrial slurries [113]. This technique is not limited by the turbidity since the measurements are based on sound rather than light propagation. O'Brien *et al.* (2003) used electroacoustic spectroscopy to successfully determine the size and zeta potential of a highly concentrated silica NP suspension (43 wt%) while the suspension was being pumped through a flow circuit [114]. Many interesting industrial applications of this technique in nanoparticle characterization were reviewed by Hunter [113]. In addition, electroacoustic spectroscopy can be used for characterization of NPs while they are embedded in opaque non-Newtonian media. Adibnia and Hill (2014) used electroacoustic spectroscopy to show that NPs embedded in hydrogel distribute heterogeneously, and reflect different diffusive patterns within sub-populations of NPs [115].

Tunable resistive pore sensing allows the analysis of size and zeta potential of individual particles in a suspension. In this technique a resistance pulse is generated over time each time individual particles pass through a pore. The pulse profile can be interpreted using appropriate theories to extract the particle size, shape, charge and concentration [116]. Evidently, the pore size dictates the size range of the particle to be analyzed. Therefore, size tunable pore sensors were introduced to tune the pore dimensions typically using mechanically stretching elastic pores [117]. Using an appropriate theoretical model, Kozak *et al.* (2012) extracted the electrophoretic component of the particle motion in the pore, and successfully evaluated the ζ-potential and size of individual polystyrene particles [117]. Vogel *et al.* implemented a high-resolution tunable resistive pulse technique to measure size and ζ-potential of biological samples such as mixed anionic, cationic liposomes and extracellular vesicles in plasma on a single particle analysis basis (see Figure 9). They also studied the *in-situ* immobilization of DNA on

magnetic particles by measuring individual particles ζ-potential [118]. Tunable resistive pulse sensing can also be used to investigate adsorbed protein layers on nanoparticles by individual particle size measurement [119], which is not possible using conventional techniques such as dynamic light scattering due to the formation of agglomerates. It should be noted that the sensitivity and throughput of resistive pulse sensing is still improving, especially with the integration of micro- and nano-fabrication technologies [120].

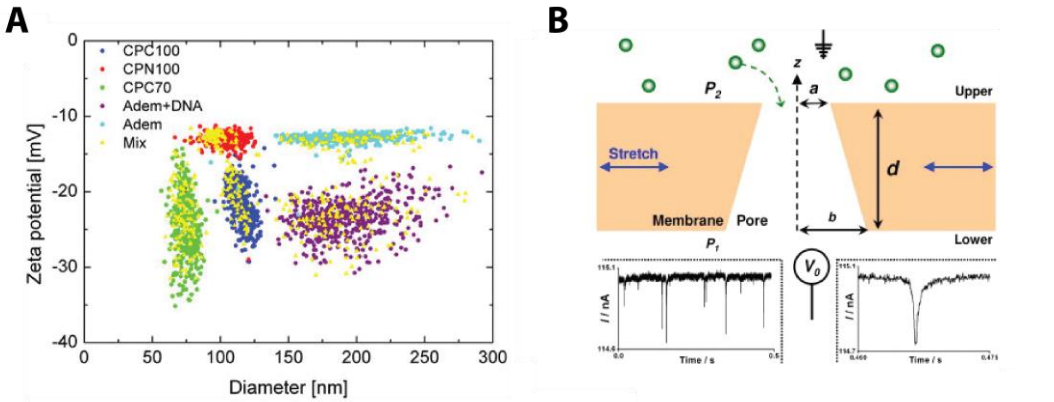

Figure 9. (A) Zeta potential vs particle size of bare polystyrene (CPN100), carboxylated polystyrene particles (CPC70, CPC100), magnetic particles (Bio-Adembeads) and magnetic particles modified with DNA. The mix of all 5 particle types (in yellow) resembles very well the particle distributions when particle types are measured separately. From reference Vogel et al. [118] (adapted and use with permission) (B) Principle of TRPS, schematic representation of a pore; right down: pulse signal generated by each individual particles. Adapted and use with permission from Sommerville et al.[121].

Flow cytometry can be used as a screening technique to quantitatively examine the adsorption of fluorescent proteins onto PEGylated microparticles (MP) surfaces. Observation of different population of fluorescent MP can demonstrate MP batch heterogeneity [122]. However, until recently the technique was not transferable to nano-sized objects, due to detection limitations. Recent developments have resulted in several

report of optimized “in house” equipment able to analyze nanoparticles and nanovesicles [123, 124]. The possibilities opened by these recent developments in the identification of NP subpopulation as a function of size, adsorbed proteins and surface properties are enormous [125-127].

Microfluidics has been used for nanoparticle separation and characterization. Microfluidic devices offer a convenient, single step and most importantly continuous particle separation, which is now very well-established for micron-sized particle sorting [128]. The electrophoretic mobility and particle size of individual Hepatitis B Virus capsids were measured in two nanofluidic 45 nm wide pores in series using resistive pulse sensing [129]. The nanofluidic fluorescence-based detection and characterization of small lipid vesicles on a single particle basis was done in a nano flow cytometer [130]. The device could count the number of fluorescent synthetic lipid vesicles down to a vesicle concentration of 170 fM also detecting binding reactions occurring at the surface of individual vesicles. This potentially could allow the detection of heterogeneities in vesicle subpopulations and identify specific biomolecules on the surface.

4.2. Detection and analysis of heterogeneity at the single particle level

Unfortunately, until now there are not many techniques allowing the study of NPs surface individually with high spatial resolution and high throughput. Surface heterogeneity at the single particle level is currently assessed by imaging techniques such as TEM, SEM, AFM and fluorescent microscopy.

Transmission and Scanning electronic microscopy (TEM and SEM) are the methods of choice to visualize particle heterogeneity at the population or single particle level. Size

and shape can be readily resolved providing that the particles are stable enough. Some insights into chemical heterogeneity can be detected if materials have different electronic density or could be stained with heavy metal salts. However, features such as PEG surface coverage cannot be readily analyzed. The limitations of imaging techniques are related to tedious and time consuming image analysis to obtain enough statistical power.

The surface heterogeneity of Poly(lactide-co-glycolide) (PLGA) NPs coated with a mixture of lecithin and 1,2-distearoyl-sn-glycero-3-phosphoethanolamine (DSPE)-N-polyethylene glycol (PEG) with NH_2 or $O\text{-}CH_3$ end-terminal groups was visualized by TEM. NPs visualization was carried out by grafting carboxylated quantum dots (QDs) to the PEG NH_2 terminal group on NPs surface. Similarly, patchy surface of MPs conjugated by gold NPs (AuNPs) was observed by TEM and SEM [131] . In both case the formation of patches on the surface of particles was demonstrated by Electronic Microscopy (EM). According to the authors this heterogeneity is related to the difference in segregation of DSPE-PEG according to difference in end-terminal group (NH_2 vs OCH_3). Even though this kind of technique provides a lot of information about surface heterogeneity, it should not be forgotten that the functionalization of the surface by QDs or AuNPs could create more surface heterogeneity due to the non-uniformity of chemical coupling reaction. Similar MPs were also synthesized using DSPE-PEG conjugated by fluorescent dye. Similarly, the patchy surface was observed on the MPs surface by confocal microscopy [131].

Surface heterogeneity of individual liposomes with diameters between 50 nm to 1.5 µm was reported by high-throughput confocal fluorescent microscopy. The labeled liposomes were prepared with a pair of fluorescent lipid analogues with identical fatty

acid tails (phospholipid DHPE and fatty acid C16 respectively) attached to two different fluorescent dyes. The molar ratio of the two labels was analyzed by confocal fluorescent microscopy on individual liposome by measuring their intensity ratio. Variable label molar ratio were recorded for individual liposomes, reflecting lipid composition heterogeneity [103]. However, because of the low resolution of confocal microscopy in the submicron range, it does not allow visualizing individual liposome surface with high enough detail.

The ratio of lipid to proteins of proteoliposome with mean diameter of 100 nm was determined by confocal fluorescent microscopy. High throughput analysis of proteoliposome was performed by labeling the transmembrane proteins with Cy3 or Cy5 and the lipid phase with Oregon green DHPE3. The analyses of thousands of proteoliposomes allowed the heterogeneity in distribution of transmembrane protein in proteoliposomes to be characterized. Three subpopulations of proteoliposomes with different transmembrane protein compositions could be identified [132]. This could have implications in formulation of targeted liposome for drug delivery using surface proteins as targeting ligand.

Atomic force microscopy (AFM) is a reliable approach to obtain information about the nanoscale heterogeneity on the surface of coated or functionalized material. AFM is frequently used to characterize NP size distribution [133-135]. However, to the best of our knowledge, in very few articles, AFM was used to study the surface properties related to the surface heterogeneity. The shape, size and core-shell structure of superparamagnetic iron oxide nanoparticles (SPION) modified by pullulan (a polysaccharide used to increase biocompatibility of SPION) was investigated by AFM. In this study, the authors

demonstrated that the particle structures is constituted of an inner magnetite core and an outer polymeric shell of pullulan [136]. The nanoscale spatial resolution of AFM provides important information about nanoparticles surface. As previously mentioned in section 2.1, heterogeneous distribution of PEG was observed in AFM topographic mode [65] or AFM "phase imaging" mode [66, 67] .

Stan *et al.* applied AFM and atomic force spectroscopy (AFS) in contact and tapping mode on flat gold substrates functionalized by PEG thiol in aqueous PEG solution. In this study, the morphology and PEG heterogeneity of surface coverage and the mechanical properties of the PEG surface coatings were measured by AFS [137]. Additionally, the data gathered by AFM and AFS provided enough statistical evidence to calculate the length and density of PEG brush. The authors reported a significant heterogeneity in PEG surface coverage, forming sparse and brush-like islands. It is important to mention that this study was performed on flat gold surfaces, and it is yet to be applied to spherical gold NPs. A similar study was performed by Nnebe *et al.* on PEG chain layer grafted on silica by tapping-mode AFM. Analyses of compression forces applied by the AFM probe on the surface PEG layer reflected the grafting density and the PEG layer thickness, which could reveal heterogeneity in surface chemistry [138].

Atomic force microscopy scanning electrochemical microscopy (AFM-SECM) was employed by Huang *et al.* to visualize the PEG corona labeled by ferrocence [139]. Additionally, AFM-SECM could allow the visualization of the gold core of individual NPs. In this technique, by generating a specific tip current, a microelectrode probe allows electrochemical detection of the PEG labeled by ferrocence (Fc-PEG redox label) immobilized onto a 20 nm gold NP surface. The intensity of this specific current relies on

the concentration of ferrocence or any other redox label on the surface of the gold NPs, while AFM tapping mode determine the location on individual NPs. In other words, AFM-SECM allows the determination of the statistical distribution of PEG density in the surface of gold NPS by analyzing individual NPs. In this study, for each image a histogram showing the distribution of the number of Fc-PEG chains per nanoparticle probed was generated. AFM-SECM could be useful to detect the surface heterogeneity within the same batch of NPs as the redox-labeled macromolecule resolution was found to be around 20 nm. However, AFM-SECM is not a universal technique as it could be applied only to NPs with conducting substrate. Additionally, the use of AFM-SECM requires the functionalization with redox label, limiting the range of application of this technique.

Structural disorders and packing efficiency of the phospholipid bilayer of giant multilamellar liposomes (diameter in the order of hundred microns) were visualized by Confocal Raman Microspectroscopy. The combination of Raman spectroscopy and microscopy allows for the mapping of the surface composition of the material with a superior resolution in the sub-micron range [140]. The authors investigated three regions in the vibrational spectrum (C-C stretching, C-H deformation and C-H stretching) to reveal phase and lateral packing heterogeneity in the phospholipid membrane. It should be mentioned that confocal Raman microspectroscopy currently cannot be applied to submicron particles because of the low spatial resolution of the technique.

A combination of different techniques is a successful approach to unveil never-seen-before surface details at the nanoscale. A good example is the combination of super-

resolution fluorescence microscopy (SRFM) with TEM techniques to investigate structure heterogeneity of soft NPs [141].

Core−shell architectures of hard and soft core/shell NP stained by fluorescent dye or AuNPs or AgNPs were visualized by SRFM (fluorescent probe) or TEM (metallic NPs). Microscopy data allows determining the 2D radial distribution of metallic NPs or fluorophores, therefore allowing the 3D reconstruction of the internal structure of the core/shell NPs [141]. This technique enables quantifying the different compartment volumes in a single microgel, and to access the quantitative evaluation of structural heterogeneity of a NP ensemble. Moreover, temperature-induced changes of the responsive soft shell labelled with AgNPs could be observed at the single microgel level [141].

Combination of AFM and infrared (IR) spectroscopy was shown to provide the high topographic spatial resolution of AFM in combination with the thermal, chemical analysis and compositional imaging capabilities of IR spectroscopy, showing great potential for NP investigation [142]. More generally, the effective characterization of particle surface homogeneity can only result from combination of methods as shown by F. Stellacci and coworkers [143].

Table 1. Methods reported for (1) Analysis at the nanoparticle suspension level (2) Analysis at single particle level.

Technique	Application	Advantage	Limitation	Reference
Analysis on suspension				
Confocal fluorescent microscopy	Direct observation of batches	Visual identification of heterogeneities	Low throughput screening Limited resolution for submicron particles Staining of surface by Fluorescent dye	[103], [131]
Capillary electrophoresis	Single particle separation and characterization	Separation along with screening	Not applicable to uncharged particles, Relatively low detection efficiency	[107], [108], [109], [110], [111]
Electroacoustic spectroscopy	NP size and charge characterization	High throughput screening, Applicable to highly concentrated samples, Continuous online characterization	Not applicable to low-density particles, Properties are measured continuously but averaged for the population at each time point	[113] , [114]
Flow cytometry	Investigating batch heterogeneity	Surface characterization is possible	Not applicable to single particle characterization	[123], [124]
Tunable resistive pore sensing	Single particle characterization	Reliable one-by-one characterization of size, surface, and electrical properties	Sensitivity and throughput is still improving	[117], [118], [119]

Micro- and nano-fluidics	NP separation and characterization	Single step continious approach. Nanofluidics applicable to single particle analysis	Low throughput screening	[128], [129], [130]
Analysis at the single particle level				
Transmission electronic microscopy (TEM)	Direct observation of NP batches	Visualisation of intact NPs	Staining of surface Sensitivity of NPs to electrons	[131]
Electrochemical atomic force microscopy	Probing surface of individual nanoparticles	High spatial resolution	Surface functionalization by redox label	[139]
Atomic force microscopy (AFM)	All types of solid particle (in air)	Ease of application	Resolution: Limited by AFM tip, Unable to determine the detailed characteristics of the morphology	[143]
Raman microspectroscopy	chemical composition mapping of particles surface	Mapping chemical composition of single particle	Limited resolution for submicron particles	[140]
Super-resolution fluorescence microscopy (SRFM)	Direct observation of NP batches	Visualisation of intact NPs	Staining of surface is necessary Diffraction-limited	[141]

4.3. Data presentation and statistical considerations in heterogeneity assessment

Parameter heterogeneity statistical assessment is of paramount importance, but a complex issue. In this section, discussion is limited to some basic issues, readers interested in more information are invited to consult suggested textbook and references cited in the following sections [144].

Data distribution and central tendency values

NP physicochemical properties can follow different statistical distributions (Figure 10). Central tendency measurements, arithmetic mean, median or mode, are often used as descriptors of NP properties, but they are insufficient to get insight into heterogeneity [63]. Indeed, the same mean could be the result of very different types of statistical distribution, as illustrated by Figure 10 A and B. Further, central tendency values can be misleading when considering outlier values in their calculation. The same argument applies to standard deviation values; if standard deviations give good insight on heterogeneity in the case of Gaussian distributions, it may not be as informative for less conventional distributions. This calls for the correct determination of the data distribution of measurements. For instance, the Poisson distribution appears to be a better fit for ligand distribution data than the Gaussian distribution, particularly when the number of ligand is low (Figure 10 C).[62, 145]

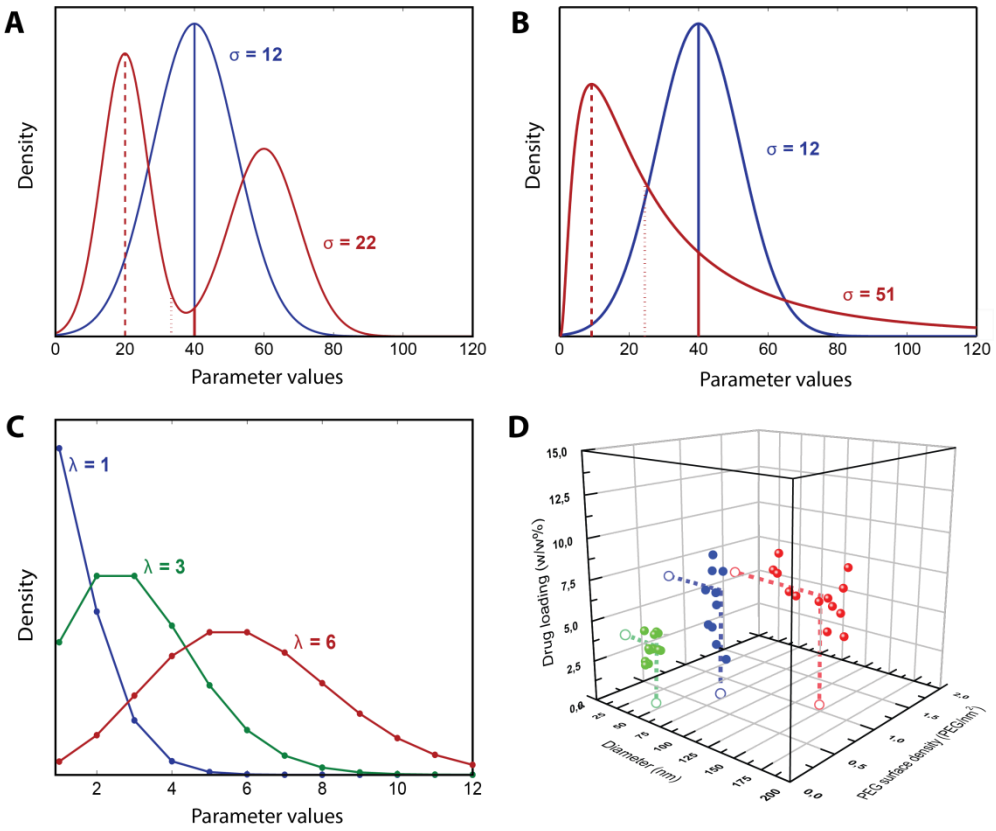

Figure 10. Statistical distributions: (A) Normal and bimodal distributions; (B) Normal and skewed distributions with central tendency values (Mean: solid line; Median: dotted line, Mode: dashed line, σ: standard deviation of the color-associated distribution), In A and B: Mean=40 for all the distribution, while mode and median are varying with the type of distribution. In the case of normal distribution: Mean=Median=Mode (C) Poison distributions-with different Poisson parameter λ (mean and variance); (D) 3D plot, a possible representation of a nanoparticle population for which 3 different parameters are known for each NP individually.

Statistical considerations regarding multiple parameters analysis

If we consider different parameters, for example size, ligand density and surface charge for the same NP suspension, the three central tendency values can give the impression that most NPs have their three parameter values close to the multivariate mean. However, this may only be the case when the parameters are both independent and follow unimodal, narrow distributions. Hence, it may be that only a small fraction of the NP suspensions displays these values for the three parameters. It is also possible that clusters of NP suspensions arise when parameters correlate (see Figure 10 D). Unless the

three parameters are measured simultaneously on the same particle and for a representative number of particle from the suspension, it cannot be assumed that an "average" nanoparticles exist [146].

In conclusion, the end-goal is to be able to determine which fraction of the suspension is having the desired targeted values for all the key parameters. In other words the goal is to determine which part of the NP distribution leads to the desired biological outcomes. Collecting information about parameter distributions, in addition to central tendency values, is important to ensure a critical number of particles have the desired properties. Ideally, this information would be gained from measurements obtained on individual particles or from careful sub population samplings. Otherwise, it would be important to find ways of estimating the percentage of NP populations having parameter values within specific interval limits, something that can be envisioned under reasonable assumptions about distributions and correlations.

5. Perspectives

5.1. Factors impacting suspension heterogeneity

The intended or unintended presence of non-uniform surface and domains on NPs usually results from the following reasons: 1) dispersity of materials properties such as size and chemical composition; 2) phase separation between two or more components of the same particle, typically lipids and/or polymers; 3) non-homogenous mixing of materials or reactants; and finally 4) incomplete chemical reactions.

Role of materials heterogeneity

In a bottom-up strategy (usual for lipid and polymer NP assembly), the structuration at the higher level of organization (the particle) strongly depends on material properties and dispersity. The materials could show dispersity in chain/block size as well as dispersity in chemical composition. The latter could result from non-homogenous monomer distribution; local fluctuation along the chain, or in the case of phospholipid materials, different fatty acids chain lengths. It is hypothesized that dispersity could affect the structuration as well as the heterogeneity of the next level of organization.

For instance, it has been shown that in some conditions a mix of block copolymer with a fraction of hydrophobic homopolymer as low as 10% w/w can trigger a change in particle morphology from vesicles to spheres [147]. This could be an issue with copolymers that are not completely purified and characterized, such as block copolymers resulting from coupling reactions [148].

On the other hand, some other studies reported contradictory results. As it was reported by Lebouille *et al.,* polymer composition and size dispersity does not have a significant influence on NPs size when prepared in a fast mixing process [149]. However, the effect of polymer dispersity on slow mixing processes has not been elucidated.

Relationship between polydispersity and self-assembly/phase separation of block copolymers has been reviewed recently [150]. As mentioned in this review, poly dispersity index (PDI) is a poor descriptor of dispersity breadth as it depends on a number-average molecular mass. Calculated molar mass dispersity (MMD) is a better descriptor of the breadth of chain distribution [150]. MMD influences almost every aspect of self-assembly, from microphase separated domains size to interface thickness and temperature at which ordered/disordered transition occurred. The influence of MMD modulation is interpreted

in terms of change in entropy of the system: 1) A decrease in entropic penalty associated with the fact that less chain stretching is required as the long chains fill the bulk of the domains while the short chains adopt relaxed conformations at interphase; 2) An increase in configurational entropy when smaller chains present in a domain with a broad MMD are pulled into the other phase separated domains. The relative contributions of these two phenomena depend on the broadness of the molecular weight distribution. This is an important issue for the industrial development of nanomaterials because industrially produced block copolymers possess higher variability than controlled laboratory produced copolymers. Polydisperse copolymers can out-perform narrow dispersed block copolymers as they can lead to new morphologies and larger nanodomains [151].

Control of nanomaterial assembly: phase separation

Self-assembly of block polymer at nanoscale is a common way to prepare complex structures with different morphologies. When diblock polymers or polymer blends are dissolved in a mixed phase (organic solvent phase), upon solvent withdrawal the mixed phase could be demixed and form a two-phase system if blocks are chemically incompatible. Block copolymers cannot separate in macroscopic scale, but they segregate locally, in microscale. The block segregation is enthalpy driven by repulsive forces between unlike chains. Phase organization strongly depends on the speed and direction of solvent removal. Different morphologies and structures could be produced if parameters of the phase separation process are slightly modified. In particular, the volume fraction of one block is an important factor in determining which structure will be adopted. Interaction parameter between blocks χ (which is temperature dependent) and the degree of polymerization of a block N are as the other effective parameters since their product

represent the segregation strength between blocks [152, 153]. For instance, a mix of closely related polyesters could lead to specific structuration: phase separation of PLGA and PCL at the wall of a polymer capsule creates PCL domains on the capsule's surface [24].

The self-assembly of material leads to the formation of only a few type of nanostructure. Recently, it has been argued that this limitation is due to a lack of information "programmed" into the starting material [154]. For instance, the nature and size of the building blocks can be seen as information to direct assembly of domains with specific shape and size [154]. It is expected that the addition of information to guide materials assembly may improve colloid homogeneity or engineered heterogeneity.

These considerations on phase separation and organization of polymer materials can also be considered with hybrid materials, mixture of lipids and polymer or other additives such as cholesterol or surfactant molecules.

Control of materials assembly: mixing

Most preparation methods involve a thermodynamic and kinetic control of material assembly[147, 155], and the mixing time plays a major role if particle assembly and organization depends on both polymer precipitation and phase separation.

Chemical engineers are well aware of the challenges related to the mixing at different time and length scales to achieve chemical reaction homogeneity and reliable end-products. Complete mixing at very short length scale, which is necessary to obtain nanoscale structures, is very difficult to achieve due to the dependence of perfect mixing to time. Incomplete micromixing coupled with non-linear chemical reactions, autocatalysis or assembly can yield to extremely variable outcomes [156].

In the context of polymer nanocarrier assembly by nanoprecipitation processes, size and size dispersity was found to be directly related to the speed and homogeneity of mixing of the solvent and anti-solvent phases. Several technological solutions have proposed such as Nanoflash micromixing and microfluidic approaches to resolve the issue of complete mixing [157-160]. These issues become more important at the scale up step, as efficient mixers are difficult to scale up.

However, when a microfluidic mixing method such as the staggered Herringbone mixing nanoprecipitation (SHMN) is compared to classical batch nanoprecipitation (BN), it is found that the process with the fastest mixing time (SHMN) produces smaller NPs with less batch-to-batch variability than BN [161]. On the other hand, size polydispersity index is greater for SHMN than BN, suggesting that size control remains a complex issue [161].

Heterogeneity due to incomplete chemical reaction and purification

Nanocarrier preparation involves several chemical reaction steps, including synthesis using the raw materials and surface modification by coupling reaction to add ligands and polymers to modify the surface. Heterogeneity could arise from incomplete chemical reaction, unavailability of reactive groups due to steric and conformation hindrances, slow reaction kinetic and difficulties to purify and homogenize the resulting modified particles. When reaction involves polymerization, inhomogeneity could arise from initiation, propagation and termination of chains [162].

Polymer-stabilized colloids can be produced by surface modification by polymer grafting. The grafting method plays an important role in the degree of homogeneity of the polymer-grafted surface. Two grafting strategies are available, the “grafting to” approach,

which is grafting polymer chains on the surface; and "grafting from" approach, which consists of direct polymerization of pendant chains from the NP surface. The "grafting from" approach has been credited for higher grafting density, thereby more homogenous surface coverage [163]. However, as demonstrated by a simulation study, the "grafting to" approach yields to NPs with a more isotropic polymer coverage and a more homogenous surface than the "grafting from" strategy [163]. On the other hand the grafting efficiency of the "grafting to" approach is a rather low, and leads to lower ligand density. Noteworthy, a recent study showed no differences in the two conjugation approaches regarding surface heterogeneity [164].

The challenges related to precisely conjugate a ligand on a scaffold have been addressed in a recent review [145]. One of the main issues when synthesizing multivalent functional conjugates is the heterogeneity of the end-product which is often a complex mixture of imaging dye, targeting ligand and active compound, all grafted on a polymer scaffold. Grafting of multiple molecules on the scaffold can lead to large numbers of different possible combinations. This was recently elegantly demonstrated in the case of stepwise conjugations of targeting ligand, active molecule and tracking dye to G5 PAMAM dendrimers which lead to over 4000 combinations of possible conjugates [145].

Surface grafting heterogeneity in Au NPs functionalized with thiolated DNA has been studied by localized surface plasmon resonance. Variations of about 10% in DNA coverage were observed in particle suspensions, a significantly higher dispersity than what was expected from a Poisson distribution (usually used for discrete data distribution). This large variation in surface coverage was attributed to the heterogeneity of particle surface properties resulting from a difference in reaction rates between

particles [165]. Another well studied case in the nanocarrier domain are dendrimer formulations, which are a complex mix of different dendrimer generations, with slightly dispersed arborescent structures, displaying different pharmacokinetics and toxicological properties [166-168].

5.2. Innate heterogeneity vs. acquired heterogeneity

When introduced in a biological media, nanocarriers experience immediate opsonisation, *i.e.,* adsorption of proteins on their surface. This process has a strong impact on toxicity, immunotoxicity, biodistribution, particle-cell interactions and drug targeting. It is now well accepted that nanocarrier fate largely depends on the amount and type of bound/adsorbed proteins at the surface of the carrier. The quantity and type of the proteins adsorbed on a NP surface depend on a number of factors related to the nanocarriers properties including chemical composition of the surface [12, 169], size [6] and topography of the surface [170], as well as factors related to the protein composition and duration of exposure [171]. The formation of the protein corona introduces a new source of heterogeneity that is only partially related to the properties of the pristine NPs.

As discussed above, a hydrophilic PEG corona can prevent protein fouling to some extent. But it can also affect protein adsorption kinetics and therefore the time evolution of the corona composition[41, 172]. On the other hand, PEG surface heterogeneity such as “bald spot” can induce rapid and local protein adsorption on a NP surface, triggering complement and/or immune system recognition cascade[6].

Opsonisation is a dynamic process as protein adsorption is the result of interplay between protein affinity and relative abundance. Moreover, complex phenomenon such as protein denaturation and cooperative binding can take place. Protein adsorption is

1 therefore highly complex and non-linear phenomena which makes prediction of the
2 corona composition extremely difficult.

3 When protein corona is analyzed, one can only report an average protein
4 composition. But this averaged composition do not necessarily reflect the real
5 composition on individual particles, as recently discussed by Forest and Pourchez [146].
6 Different protein distributions for the same average protein composition are
7 schematically illustrated in Figure 11. It can be envisioned that these different
8 distributions can produce very different outcomes regarding toxicity, ligand recognition,
9 biodistribution and drug delivery efficacy.

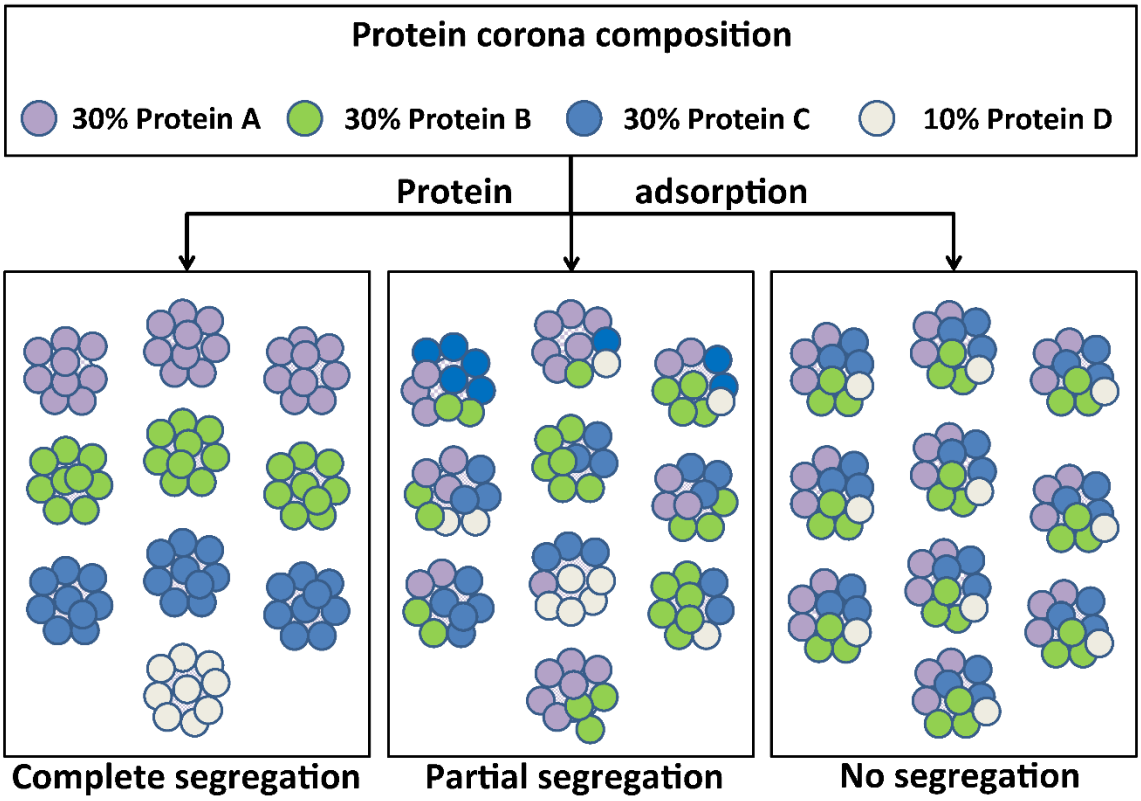

10

11 *Figure 11. Possible scenarios after proteomic analysis of the protein corona of a*
12 *suspension of 10 NPs with the same average composition. Adapted from [146] with*
13 *permission.*

14

Precise characterization of the protein corona heterogeneity requires analytical techniques able to quantify the protein corona composition at the single particle level. Some attempt have been reported using differential centrifugal sedimentation, showing that the protein corona composition depends strongly on NP size, with larger particles being more prone to protein adsorption [173]. Spatial localization of proteins on NP surface has been characterized using a combination of antibody-labelled gold NPs, differential centrifugal sedimentation and various imaging techniques as well[174]. The spatial organization of epitope (adsorbed transferrin) at the surface of the NPs was found to be random, consistent with a random protein adsorption for this protein [174].

Protein adsorption on mesoporous silica NPs was investigated on individual particle by stochastic optical reconstruction microscopy (STORM) [175]. STORM has a spatial resolution in the 20 nm range allowing quantification and visualization of adsorbed proteins. The study showed that protein adsorption was highly heterogeneous inside the same NP suspension and evolved with time. The authors speculated that small differences in surface chemistry were resulting in different protein adsorption pattern amplifying particle diversity and resulting in the coexistence of particles with very different protein layers [175]. In spite of these recent advances, at this time the technical challenges related to corona heterogeneity investigation are still ahead of us.

Conclusions and outlook

In this review we intent to raise awareness about the importance of nanomaterial heterogeneity and its so far known consequences, especially in the biomedical field. We

provide some guidelines to identify and to analyze it, and we explore the possibility of controlling it through experiments aimed at creating heterogeneous systems.

It could be understood, in a bioengineering and regulatory perspective, that obtaining homogenous NPs is important to obtain predictable, reproducible and fully functional NP batches. Indeed, variations in key chemical surface properties such as PEG coverage and ligand grafting density are contributing to the reduction of the effective dose of drug nanocarrier with the optimal properties within the same particle suspension. As discussed by Forest and Pourchez in their paper "the myth of the average nanoparticle", a ligand functionalized PEGylated nanocarrier displaying the average size, ligand and PEG densities may not exist in the actual NP batch as the average values may hide extreme values for each of these parameters [146]. A similar issue is arising from synthesis of multivalent functional conjugates, comprising tracking dye, targeting ligand and active grafted on a polymer scaffold [145].

Even though nanocarriers heterogeneity is a known problem, it is difficult to tackle as most measurements are still performed on a NPs ensemble, instead of on subpopulations/fractions or individual particles. There is an urgent need to develop methods to study particle sub-population heterogeneity and single particle heterogeneity. It can be expected that present and future developments of combination of analytical techniques and computational modelling of NPs structures could provide with new insights into the heterogeneity phenomena. Lately, strong efforts towards reaching this goal have been made with the development of the "Nanotechnology Characterization Laboratory" in the USA (https://ncl.cancer.gov/) and recently in the EU

(http://www.euncl.eu/). These laboratories contribute to standardized procedures to fully characterize nanomaterials.

On the other hand, heterogeneous (and eventually irregular) surfaces, such as patchy surfaces, may provide unprecedented properties for drug delivery. Heterogeneity can be beneficial if it is implemented in a controlled fashion among the entire NP population. Otherwise, it often results in unpredictable and adverse effects in different applications. The current trend toward biomimetic strategies boosts the interest for nanocarriers with surface heterogeneity. Indeed, biological membranes are complex mixtures of lipids proteins and proteoglycans, forming at the same time a very well structured and heterogeneous interface, which fulfills complex functions. Biomimetic strategies include the addition of a plasmatic membrane on NP surface [176, 177], elaboration of mimetic of lipoprotein [178], or pathogen mimetics amongst other[179].

In concrete terms, a practical course of action should include a more scrutinized determination of the statistical distribution of data to get an in-depth understanding of the NP batch characteristics. This can be done using existing analytical techniques, using extensive sample fractionation to get information on sampled subpopulations, improving resolution of analytical techniques (such as flow cytometry), combining techniques in order to get better insights into chemical data, and to get simultaneous information on the same NPs. At the same time we ought to be able to make more connections between this newly documented NP heterogeneity and biological outcomes, such as targeting, biodistribution, ability to diffuse in biological media and therapeutic efficacy.

Conflicts of interest

The authors declare no conflict of interest

Acknowledgments

JMR gratefully acknowledge postdoctoral funding by NSERC/CRSNG (Government of Canada), XB is grateful for the financial support from the CRC program. CR is grateful for the financial support from the Louise and André Charon Research Chair in Alzheimer disease (INRS, Fondation Universitaire Armand-Frappier), PH and XB acknowledge support from NSERC/CRSNG "Discovery grant program".

References

1. J. Fang, H. Nakamura and H. Maeda, *Adv Drug Deliv Rev*, 2011, **63**, 136-151.
2. Y. H. Bae and K. Park, *Journal of Controlled Release*, 2011, **153**, 198-205.
3. D. J. A. Crommelin and A. T. Florence, *International Journal of Pharmaceutics*, 2013.
4. S. Wilhelm, A. J. Tavares, Q. Dai, S. Ohta, J. Audet, H. F. Dvorak and W. C. W. Chan, *Nature Reviews Materials*, 2016, **1**, 16014.
5. S. D. Perrault, C. Walkey, T. Jennings, H. C. Fischer and W. C. Chan, *Nano Lett*, 2009, **9**, 1909-1915.
6. A. Vonarbourg, C. Passirani, P. Saulnier and J. P. Benoit, *Biomaterials*, 2006, **27**, 4356-4373.
7. M. V. D. Z. Park, A. M. Neigh, J. P. Vermeulen, L. J. J. de la Fonteyne, H. W. Verharen, J. J. Briedé, H. van Loveren and W. H. de Jong, *Biomaterials*, 2011, **32**, 9810-9817.
8. X.-D. Zhang, D. Wu, X. Shen, P.-X. Liu, N. Yang, B. Zhao, H. Zhang, Y.-M. Sun, L.-A. Zhang and F.-Y. Fan, *International Journal of Nanomedicine*, 2011, **6**, 2071-2081.
9. I. M. Adjei, C. Peetla and V. Labhasetwar, *Nanomedicine*, 2013, DOI: 10.2217/nnm.13.70, 1-12.
10. J. W. Hickey, J. L. Santos, J.-M. Williford and H.-Q. Mao, *Journal of Controlled Release*, 2015, **219**, 536-547.
11. J.-B. Coty and C. Vauthier, *Journal of Controlled Release*, 2018, **275**, 254-268.

12. E. S. Melby, S. E. Lohse, J. E. Park, A. M. Vartanian, R. A. Putans, H. B. Abbott, R. J. Hamers, C. J. Murphy and J. A. Pedersen, *ACS Nano*, 2017, **11**, 5489-5499.
13. A. Verma, O. Uzun, Y. Hu, Y. Hu, H.-S. Han, N. Watson, S. Chen, D. J. Irvine and F. Stellacci, *Nat. Mater.*, 2008, **7**, 588-595.
14. Y. Li, X. Zhang and D. Cao, *Soft Matter*, 2014, **10**, 6844-6856.
15. Z. Cheng, A. Al Zaki, J. Z. Hui, V. R. Muzykantov and A. Tsourkas, *Science*, 2012, **338**, 903-910.
16. L. Shang, K. Nienhaus and G. U. Nienhaus, *Journal of Nanobiotechnology*, 2014, **12**, 5-5.
17. J. Wang, W. Mao, L. L. Lock, J. Tang, M. Sui, W. Sun, H. Cui, D. Xu and Y. Shen, *ACS Nano*, 2015, **9**, 7195-7206.
18. K. G. Reuter, J. L. Perry, D. Kim, J. C. Luft, R. Liu and J. M. DeSimone, *Nano Letters*, 2015, **15**, 6371-6378.
19. S. Prabha, W.-Z. Zhou, J. Panyam and V. Labhasetwar, *International Journal of Pharmaceutics*, 2002, **244**, 105-115.
20. J. Du and R. K. O'Reilly, *Chemical Society Reviews*, 2011, **40**, 2402-2416.
21. S. Ravaine and E. Duguet, *Current Opinion in Colloid & Interface Science*, 2017, **30**, 45-53.
22. Z. Poon, S. Chen, A. C. Engler, H.-i. Lee, E. Atas, G. von Maltzahn, S. N. Bhatia and P. T. Hammond, *Angewandte Chemie International Edition*, 2010, **49**, 7266-7270.
23. L. S. Grundy, V. E. Lee, N. Li, C. Sosa, W. D. Mulhearn, R. Liu, R. A. Register, A. Nikoubashman, R. K. Prud'homme, A. Z. Panagiotopoulos and R. D. Priestley, *ACS Nano*, 2018, **12**, 4660-4668.
24. W. Shi and D. A. Weitz, *Macromolecules*, 2017, **50**, 7681-7686.
25. K. Oglęcka, P. Rangamani, B. Liedberg, R. S. Kraut and A. N. Parikh, *eLife*, 2014, **3**, e03695.
26. J. Nam, T. K. Vanderlick and P. A. Beales, *Soft Matter*, 2012, **8**, 7982-7988.
27. C. LoPresti, M. Massignani, C. Fernyhough, A. Blanazs, A. J. Ryan, J. Madsen, N. J. Warren, S. P. Armes, A. L. Lewis, S. Chirasatitsin, A. J. Engler and G. Battaglia, *ACS Nano*, 2011, **5**, 1775-1784.
28. J. D. Robertson, L. Rizzello, M. Avila-Olias, J. Gaitzsch, C. Contini, M. S. Magoń, S. A. Renshaw and G. Battaglia, *Scientific Reports*, 2016, **6**, 27494.
29. J. Zhang, Y. Pei, H. Zhang, L. Wang, L. Arrington, Y. Zhang, A. Glass and A. M. Leone, *Molecular Pharmaceutics*, 2012, **10**, 397-405.
30. B. W. J. Pirok, N. Abdulhussain, T. Aalbers, B. Wouters, R. A. H. Peters and P. J. Schoenmakers, *Analytical Chemistry*, 2017, **89**, 9167-9174.
31. S. K. Sahoo, J. Panyam, S. Prabha and V. Labhasetwar, *Journal of Controlled Release*, 2002, **82**, 105-114.
32. L. Araujo, R. Löbenberg and J. Kreuter, *Journal of Drug Targeting*, 1999, **6**, 373-385.
33. B. Petri, A. Bootz, A. Khalansky, T. Hekmatara, R. Müller, R. Uhl, J. Kreuter and S. Gelperina, *Journal of Controlled Release*, 2007, **117**, 51-58.
34. D. Dutta, M. Salifu, R. W. Sirianni and S. E. Stabenfeldt, *Journal of Biomedical Materials Research Part A*, 2016, **104**, 688-696.

35. W. Chen, A. Palazzo, W. E. Hennink and R. J. Kok, *Molecular Pharmaceutics*, 2017, **14**, 459-467.
36. M. Abdulkarim, N. Agullo, B. Cattoz, P. Griffiths, A. Bernkop-Schnurch, S. Borros and M. Gumbleton, *Eur. J. Pharm. Biopharm.*, 2015, **97**, 230-238.
37. Leon D. Li, T. Crouzier, A. Sarkar, L. Dunphy, J. Han and K. Ribbeck, *Biophysical Journal*, 2013, **105**, 1357-1365.
38. J.-M. Rabanel, P. Hildgen and X. Banquy, *Journal of Controlled Release*, 2014, **185**, 71-87.
39. P. G. Degennes, *Macromolecules*, 1980, **13**, 1069-1075.
40. S. Alexander, *J. Phys. France*, 1977, **38**, 983-987.
41. N. Bertrand, P. Grenier, M. Mahmoudi, E. M. Lima, E. A. Appel, F. Dormont, J.-M. Lim, R. Karnik, R. Langer and O. C. Farokhzad, *Nature Communications*, 2017, **8**, 777.
42. T. Ishida, M. Harada, X. Y. Wang, M. Ichihara, K. Irimura and H. Kiwada, *Journal of Controlled Release*, 2005, **105**, 305-317.
43. Q. Xu, L. M. Ensign, N. J. Boylan, A. Schön, X. Gong, J.-C. Yang, N. W. Lamb, S. Cai, T. Yu, E. Freire and J. Hanes, *ACS Nano*, 2015, **9**, 9217-9227.
44. S. Zhang, C. Tang and C. Yin, *Drug Delivery*, 2015, **22**, 182-190.
45. I. Fukuda, S. Mochizuki and K. Sakurai, *Colloids and Surfaces B: Biointerfaces*, 2016, **146**, 642-648.
46. S. M. Moghimi, *Biochimica et Biophysica Acta (BBA) - Molecular Cell Research*, 2002, **1590**, 131-139.
47. J. K. Gbadamosi, A. C. Hunter and S. M. Moghimi, *FEBS Letters*, 2002, **532**, 338-344.
48. W. T. E. Bosker, P. A. Iakovlev, W. Norde and M. A. Cohen Stuart, *Journal of Colloid and Interface Science*, 2005, **286**, 496-503.
49. K. Uchida, H. Otsuka, M. Kaneko, K. Kataoka and Y. Nagasaki, *Analytical Chemistry*, 2005, **77**, 1075-1080.
50. K. Uchida, Y. Hoshino, A. Tamura, K. Yoshimoto, S. Kojima, K. Yamashita, I. Yamanaka, H. Otsuka, K. Kataoka and Y. Nagasaki, *Biointerphases*, 2007, **2**, 126-130.
51. Y. Nagasaki, *Polym J*, 2011, **43**, 949-958.
52. Y. Sadzuka, A. Nakade, R. Hirama, A. Miyagishima, Y. Nozawa, S. Hirota and T. Sonobe, *International Journal of Pharmaceutics*, 2002, **238**, 171-180.
53. Y. Sadzuka, I. Sugiyama, T. Tsuruda and T. Sonobe, *International Journal of Pharmaceutics*, 2006, **312**, 83-89.
54. T. Liu and B. Thierry, *Langmuir*, 2012, **28**, 15634-15642.
55. M. Matsumoto, M. Matsusaki and M. Akashi, *Macromolecular Bioscience*, 2014, **14**, 142-150.
56. R. Weissleder, K. Kelly, E. Y. Sun, T. Shtatland and L. Josephson, *Nature Biotechnology*, 2005, **23**, 1418.
57. K. F. Pirollo and E. H. Chang, *Trends in Biotechnology*, 2008, **26**, 552-558.
58. S. Hong, P. R. Leroueil, I. J. Majoros, B. G. Orr, J. R. Baker and M. M. Banaszak Holl, *Chemistry & Biology*, 2007, **14**, 107-115.
59. A. M. Smith, K. A. Johnston, S. E. Crawford, L. E. Marbella and J. E. Millstone, *Analyst*, 2017, **142**, 11-29.

60. M. E. Gindy, S. Ji, T. R. Hoye, A. Z. Panagiotopoulos and R. K. Prud'homme, *Biomacromolecules*, 2008, **9**, 2705-2711.
61. D. R. Elias, A. Poloukhtine, V. Popik and A. Tsourkas, *Nanomedicine: Nanotechnology, Biology and Medicine*, 2013, **9**, 194-201.
62. D. G. Mullen and M. M. Banaszak Holl, *Accounts of Chemical Research*, 2011, **44**, 1135-1145.
63. D. G. Mullen, M. Fang, A. Desai, J. R. Baker, B. G. Orr and M. M. Banaszak Holl, *ACS Nano*, 2010, **4**, 657-670.
64. R. Michel, S. Pasche, M. Textor and D. G. Castner, *Langmuir*, 2005, **21**, 12327-12332.
65. J. C. Zillies, K. Zwiorek, G. Winter and C. Coester, *Analytical Chemistry*, 2007, **79**, 4574-4580.
66. S. Sant, S. Poulin and P. Hildgen, *J Biomed Mater Res A*, 2008, **87A**, 885-895.
67. S. Essa, J. M. Rabanel and P. Hildgen, *International Journal of Pharmaceutics*, 2010, **388**, 263-273.
68. F. Bedu-Addo, P. Tang, Y. Xu and L. Huang, *Pharm Res*, 1996, **13**, 710-717.
69. J. Y. Lehtonen and P. K. Kinnunen, *Biophysical Journal*, 1995, **68**, 525-535.
70. V. Agmo Hernández, G. Karlsson and K. Edwards, *Langmuir*, 2011, **27**, 4873-4883.
71. X. Xia, M. Yang, Y. Wang, Y. Zheng, Q. Li, J. Chen and Y. Xia, *ACS Nano*, 2011, **6**, 512-522.
72. W. J. Duncanson, M. A. Figa, K. Hallock, S. Zalipsky, J. A. Hamilton and J. Y. Wong, *Biomaterials*, 2007, **28**, 4991-4999.
73. R. Hennig, K. Pollinger, A. Veser, M. Breunig and A. Goepferich, *Journal of Controlled Release*, 2014, **194**, 20-27.
74. L. Xu, J. Betker, H. Yin and T. J. Anchordoquy, *Journal of Controlled Release*, 2012, **160**, 57-63.
75. Z. Cheng, D. R. Elias, N. P. Kamat, E. D. Johnston, A. Poloukhtine, V. Popik, D. A. Hammer and A. Tsourkas, *Bioconjugate Chemistry*, 2011, **22**, 2021-2029.
76. T. P. T. Dao, F. Fernandes, M. Er-Rafik, R. Salva, M. Schmutz, A. Brûlet, M. Prieto, O. Sandre and J. F. Le Meins, *ACS Macro Letters*, 2015, **4**, 182-186.
77. E. Moradi, D. Vllasaliu, M. Garnett, F. Falcone and S. Stolnik, *RSC Advances*, 2012, **2**, 3025-3033.
78. A. B. Pawar and I. Kretzschmar, *Macromolecular Rapid Communications*, 2010, **31**, 150-168.
79. Y. Liu, B. Liu and Z. Nie, *Nano Today*, 2015, **10**, 278-300.
80. R. M. Choueiri, E. Galati, H. Thérien-Aubin, A. Klinkova, E. M. Larin, A. Querejeta-Fernández, L. Han, H. L. Xin, O. Gang, E. B. Zhulina, M. Rubinstein and E. Kumacheva, *Nature*, 2016, **538**, 79.
81. X. Ye, Z.-W. Li, Z.-Y. Sun and B. Khomami, *ACS Nano*, 2016, **10**, 5199-5203.
82. A. H. Gröschel, F. H. Schacher, H. Schmalz, O. V. Borisov, E. B. Zhulina, A. Walther and A. H. E. Müller, *Nature Communications*, 2012, **3**, 710.
83. A. H. Gröschel, A. Walther, T. I. Löbling, F. H. Schacher, H. Schmalz and A. H. E. Müller, *Nature*, 2013, **503**, 247.
84. T. I. Löbling, O. Borisov, J. S. Haataja, O. Ikkala, A. H. Gröschel and A. H. E. Müller, *Nature Communications*, 2016, **7**, 12097.

85. M. Massignani, C. LoPresti, A. Blanazs, J. Madsen, S. P. Armes, A. L. Lewis and G. Battaglia, *Small*, 2009, **5**, 2424-2432.
86. J. R. Howse, R. A. L. Jones, A. J. Ryan, T. Gough, R. Vafabakhsh and R. Golestanian, *Physical Review Letters*, 2007, **99**, 048102.
87. Z. I. Imam, L. E. Kenyon, G. Ashby, F. Nagib, M. Mendicino, C. Zhao, A. K. Gadok and J. C. Stachowiak, *Cellular and Molecular Bioengineering*, 2017, **10**, 387-403.
88. Y. Yi, L. Sanchez, Y. Gao, K. Lee and Y. Yu, *Chemistry of Materials*, 2017, **29**, 1448-1460.
89. H. Gao, J. Xiong, T. Cheng, J. Liu, L. Chu, J. Liu, R. Ma and L. Shi, *Biomacromolecules*, 2013, **14**, 460-467.
90. M. Penna, K. Ley, S. Maclaughlin and I. Yarovsky, *Faraday Discussions*, 2016, **191**, 435-464.
91. L. Shen and J. Zhu, *Advances in Colloid and Interface Science*, 2016, **228**, 40-54.
92. L.-T.-C. Tran, S. Lesieur and V. Faivre, *Expert Opinion on Drug Delivery*, 2014, **11**, 1061-1074.
93. M. Wagner, S. Holzschuh, A. Traeger, A. Fahr and U. S. Schubert, *Analytical Chemistry*, 2014, **86**, 5201-5210.
94. A. Zattoni, B. Roda, F. Borghi, V. Marassi and P. Reschiglian, *Journal of Pharmaceutical and Biomedical Analysis*, 2014, **87**, 53-61.
95. L. F. Pease, D. I. Lipin, D.-H. Tsai, M. R. Zachariah, L. H. L. Lua, M. J. Tarlov and A. P. J. Middelberg, *Biotechnology and Bioengineering*, 2009, **102**, 845-855.
96. K. L. Planken and H. Colfen, *Nanoscale*, 2010, **2**, 1849-1869.
97. C. Vauthier, C. Schmidt and P. Couvreur, *Journal of Nanoparticle Research*, 1999, **1**, 411-418.
98. C.-Y. Wen, M. Tang, J. Hu, L.-L. Wu, D.-W. Pang, J.-B. Zeng and X.-Y. Li, *Analytical Chemistry*, 2016, **88**, 10134-10142.
99. D. N. Benoit, H. Zhu, M. H. Lilierose, R. A. Verm, N. Ali, A. N. Morrison, J. D. Fortner, C. Avendano and V. L. Colvin, *Analytical Chemistry*, 2012, **84**, 9238-9245.
100. B. Demeler, T.-L. Nguyen, G. E. Gorbet, V. Schirf, E. H. Brookes, P. Mulvaney, A. a. O. El-Ballouli, J. Pan, O. M. Bakr, A. K. Demeler, B. I. Hernandez Uribe, N. Bhattarai and R. L. Whetten, *Analytical Chemistry*, 2014, **86**, 7688-7695.
101. D. Mehn, P. Iavicoli, N. Cabaleiro, S. E. Borgos, F. Caputo, O. Geiss, L. Calzolai, F. Rossi and D. Gilliland, *International Journal of Pharmaceutics*, 2017, **523**, 320-326.
102. M. Tobio, R. Gref, A. Sanchez, R. Langer and M. J. Alonso, *Pharm Res*, 1998, **15**, 270-275.
103. J. Larsen, N. S. Hatzakis and D. Stamou, *Journal of the American Chemical Society*, 2011, **133**, 10685-10687.
104. T. L. Doane, Y. Cheng, A. Babar, R. J. Hill and C. Burda, *J Am Chem Soc*, 2010, **132**, 15624-15631.
105. T. J. Daou, L. Li, P. Reiss, V. Josserand and I. Texier, *Langmuir*, 2009, **25**, 3040-3044.
106. Y. Liu, M. K. Shipton, J. Ryan, E. D. Kaufman, S. Franzen and D. L. Feldheim, *Analytical Chemistry*, 2007, **79**, 2221-2229.

107. U. Pyell, *Electrophoresis*, 2010, **31**, 814-831.
108. K. R. Riley, S. Liu, G. Yu, K. Libby, R. Cubicciotti and C. L. Colyer, *Journal of Chromatography A*, 2016, **1463**, 169-175.
109. L. Trapiella-Alfonso, F. d'Orlyé and A. Varenne, *Analytical and Bioanalytical Chemistry*, 2016, **408**, 2669-2675.
110. C. F. Duffy, A. A. McEathron and E. A. Arriaga, *ELECTROPHORESIS*, 2002, **23**, 2040-2047.
111. Y. H. Rezenom, A. D. Wellman, L. Tilstra, C. D. Medley and S. D. Gilman, *Analyst*, 2007, **132**, 1215-1222.
112. M. R. Ivanov, H. R. Bednar and A. J. Haes, *ACS Nano*, 2009, **3**, 386-394.
113. R. J. Hunter, *Colloids and Surfaces A: Physicochemical and Engineering Aspects*, 2001, **195**, 205-214.
114. R. W. O'Brien, A. Jones and W. N. Rowlands, *Colloids and Surfaces A: Physicochemical and Engineering Aspects*, 2003, **218**, 89-101.
115. V. Adibnia and R. J. Hill, *Macromolecules*, 2014, **47**, 8064-8071.
116. D. Kozak, W. Anderson, R. Vogel and M. Trau, *Nano Today*, 2011, **6**, 531-545.
117. D. Kozak, W. Anderson, R. Vogel, S. Chen, F. Antaw and M. Trau, *ACS Nano*, 2012, **6**, 6990-6997.
118. R. Vogel, A. K. Pal, S. Jambhrunkar, P. Patel, S. S. Thakur, E. Reátegui, H. S. Parekh, P. Saá, A. Stassinopoulos and M. F. Broom, *Scientific Reports*, 2017, **7**, 17479.
119. A. Sikora, A. G. Shard and C. Minelli, *Langmuir*, 2016, **32**, 2216-2224.
120. Y. Song, J. Zhang and D. Li, *Micromachines*, 2017, **8**, 204.
121. J. A. Somerville, G. R. Willmott, J. Eldridge, M. Griffiths and K. M. McGrath, *Journal of Colloid and Interface Science*, 2013, **394**, 243-251.
122. A. Chen, D. Kozak, B. J. Battersby and M. Trau, *Biofouling*, 2008, **24**, 267-273.
123. C. Chen, S. Zhu, S. Wang, W. Zhang, Y. Cheng and X. Yan, *ACS Applied Materials & Interfaces*, 2017, **9**, 13913-13919.
124. L. Yang, S. Zhu, W. Hang, L. Wu and X. Yan, *Analytical Chemistry*, 2009, **81**, 2555-2563.
125. G. Marcoux, A.-C. Duchez, N. Cloutier, P. Provost, P. A. Nigrovic and E. Boilard, *Scientific Reports*, 2016, **6**, 35928.
126. S. A. Stoner, E. Duggan, D. Condello, A. Guerrero, J. R. Turk, P. K. Narayanan and J. P. Nolan, *Cytometry Part A*, 2016, **89**, 196-206.
127. E. J. van der Vlist, E. N. M. Nolte-'t Hoen, W. Stoorvogel, G. J. A. Arkesteijn and M. H. M. Wauben, *Nature Protocols*, 2012, **7**, 1311.
128. T. Salafi, K. K. Zeming and Y. Zhang, *Lab on a Chip*, 2017, **17**, 11-33.
129. Z. D. Harms, D. G. Haywood, A. R. Kneller, L. Selzer, A. Zlotnick and S. C. Jacobson, *Analytical Chemistry*, 2015, **87**, 699-705.
130. R. Friedrich, S. Block, M. Alizadehheidari, S. Heider, J. Fritzsche, E. K. Esbjorner, F. Westerlund and M. Bally, *Lab on a Chip*, 2017, **17**, 830-841.
131. C. Salvador-Morales, P. M. Valencia, W. Gao, R. Karnik and O. C. Farokhzad, *Small*, 2013, **9**, 511-517.
132. S. Mathiasen, S. M. Christensen, J. J. Fung, S. G. F. Rasmussen, J. F. Fay, S. K. Jorgensen, S. Veshaguri, D. L. Farrens, M. Kiskowski, B. Kobilka and D. Stamou, *Nature Methods*, 2014, **11**, 931.

133. A.-Y. Jee and M. Lee, *Current Applied Physics*, 2009, **9**, e144-e147.
134. R. D. Boyd, S. K. Pichaimuthu and A. Cuenat, *Colloids and Surfaces A: Physicochemical and Engineering Aspects*, 2011, **387**, 35-42.
135. C. M. Hoo, N. Starostin, P. West and M. L. Mecartney, *Journal of Nanoparticle Research*, 2008, **10**, 89-96.
136. A. K. Gupta and M. Gupta, *Biomaterials*, 2005, **26**, 1565-1573.
137. G. Stan, F. W. DelRio, R. I. MacCuspie and R. F. Cook, *The Journal of Physical Chemistry B*, 2012, **116**, 3138-3147.
138. I. M. Nnebe and J. W. Schneider, *Macromolecules*, 2006, **39**, 3616-3621.
139. K. Huang, A. Anne, M. A. Bahri and C. Demaille, *ACS Nano*, 2013, **7**, 4151-4163.
140. H. Noothalapati, K. Iwasaki, C. Yoshimoto, K. Yoshikiyo, T. Nishikawa, M. Ando, H.-o. Hamaguchi and T. Yamamoto, *Spectrochimica Acta Part A: Molecular and Biomolecular Spectroscopy*, 2017, **187**, 186-190.
141. A. P. H. Gelissen, A. Oppermann, T. Caumanns, P. Hebbeker, S. K. Turnhoff, R. Tiwari, S. Eisold, U. Simon, Y. Lu, J. Mayer, W. Richtering, A. Walther and D. Wöll, *Nano Letters*, 2016, **16**, 7295-7301.
142. A. Dazzi and C. B. Prater, *Chemical Reviews*, 2017, **117**, 5146-5173.
143. Q. Ong, Z. Luo and F. Stellacci, *Accounts of Chemical Research*, 2017, **50**, 1911-1919.
144. Catherine Forbes, Merran Evans, Nicholas Hastings and B. Peacock, *Statistical Distributions, 4th edition*, John Wiley & Sons, Inc., 2010.
145. M. A. van Dongen, C. A. Dougherty and M. M. Banaszak Holl, *Biomacromolecules*, 2014, **15**, 3215-3234.
146. V. Forest and J. Pourchez, *Nano Today*, 2016, **11**, 700-703.
147. Y. Mai and A. Eisenberg, *Chemical Society Reviews*, 2012, **41**, 5969-5985.
148. S. Marrache and S. Dhar, *Proceedings of the National Academy of Sciences*, 2012, **109**, 16288-16293.
149. J. G. J. L. Lebouille, R. Stepanyan, J. J. M. Slot, M. A. Cohen Stuart and R. Tuinier, *Colloids and Surfaces A: Physicochemical and Engineering Aspects*, 2014, **460**, 225-235.
150. N. A. Lynd, A. J. Meuler and M. A. Hillmyer, *Progress in Polymer Science*, 2008, **33**, 875-893.
151. K. Matyjaszewski, *Science*, 2011, **333**, 1104-1105.
152. F. Bates, *Science*, 1991, **251**, 898-905.
153. L. Leibler, *Macromolecules*, 1980, **13**, 1602-1617.
154. L. Cademartiri and K. J. M. Bishop, *Nat. Mater.*, 2015, **14**, 2-9.
155. C. Allen, D. Maysinger and A. Eisenberg, *Colloids and Surfaces B: Biointerfaces*, 1999, **16**, 3-27.
156. I. R. Epstein, *Nature*, 1995, **374**, 321.
157. R. Karnik, F. Gu, P. Basto, C. Cannizzaro, L. Dean, W. Kyei-Manu, R. Langer and O. C. Farokhzad, *Nano Letters*, 2008, **8**, 2906-2912.
158. S. P. Kee and A. Gavriilidis, *Chem Eng J*, 2008, **142**, 109-121.
159. A. D. Stroock, S. K. W. Dertinger, A. Ajdari, I. Mezić, H. A. Stone and G. M. Whitesides, *Science*, 2002, **295**, 647-651.

160. S. M. D'addio and R. K. Prud'homme, *Advanced drug delivery reviews*, 2011, **63**, 417-426.
161. T. R. García, A. G. Ac, A. Lalloz, F.-X. Lacasse, P. Hildgen, J.-M. Rabanel and X. Banquy, *Langmuir*, 2018, **34**, pp 5772–5780.
162. C. M. Hui, J. Pietrasik, M. Schmitt, C. Mahoney, J. Choi, M. R. Bockstaller and K. Matyjaszewski, *Chemistry of Materials*, 2014, **26**, 745-762.
163. M. Asai, D. Zhao and S. K. Kumar, *ACS Nano*, 2017, **11**, 7028-7035.
164. H. Liu, H.-Y. Zhao, F. Müller-Plathe, H.-J. Qian, Z.-Y. Sun and Z.-Y. Lu, *Macromolecules*, 2018, DOI: 10.1021/acs.macromol.8b00309.
165. M. Horáček, R. E. Armstrong and P. Zijlstra, *Langmuir*, 2018, **34**, 131-138.
166. M. A. van Dongen, A. Desai, B. G. Orr, J. R. Baker and M. M. Banaszak Holl, *Polymer*, 2013, **54**, 4126-4133.
167. I. Elkin, X. Banquy, C. J. Barrett and P. Hildgen, *Journal of Controlled Release*, 2017, **264**, 288-305.
168. X. Shi, I. J. Majoros, A. K. Patri, X. Bi, M. T. Islam, A. Desai, T. R. Ganser and J. J. R. Baker, *Analyst*, 2006, **131**, 374-381.
169. M. Lundqvist, J. Stigler, G. Elia, I. Lynch, T. Cedervall and K. A. Dawson, *P Natl Acad Sci USA*, 2008, **105**, 14265-14270.
170. R. X. Huang, R. R. Carney, K. Ikuma, F. Stellacci and B. L. T. Lau, *Acs Nano*, 2014, **8**, 5402-5412.
171. M. Mahmoudi, N. Bertrand, H. Zope and O. C. Farokhzad, *Nano Today*, 2016, **11**, 817-832.
172. S. Schöttler, G. Becker, S. Winzen, T. Steinbach, K. Mohr, K. Landfester, V. Mailänder and F. R. Wurm, *Nature Nanotechnology*, 2016, **11**, 372.
173. R. Wang, L. Chen, D. Li, R. Liu and G. Ge, *Particle & Particle Systems Characterization*, 2017, **34**, 1770040-n/a.
174. P. M. Kelly, C. Åberg, E. Polo, A. O'Connell, J. Cookman, J. Fallon, Ž. Krpetić and K. A. Dawson, *Nature Nanotechnology*, 2015, **10**, 472.
175. N. Feiner-Gracia, M. Beck, S. Pujals, S. Tosi, T. Mandal, C. Buske, M. Linden and L. Albertazzi, *Small*, 2017, **13**, 1701631-n/a.
176. C.-M. J. Hu, L. Zhang, S. Aryal, C. Cheung, R. H. Fang and L. Zhang, *Proceedings of the National Academy of Sciences*, 2011, **108**, 10980-10985.
177. B. T. Luk and L. Zhang, *Journal of Controlled Release*, 2015, **220**, 600-607.
178. Q. Song, M. Huang, L. Yao, X. Wang, X. Gu, J. Chen, J. Chen, J. Huang, Q. Hu, T. Kang, Z. Rong, H. Qi, G. Zheng, H. Chen and X. Gao, *ACS Nano*, 2014, **8**, 2345-2359.
179. J.-W. Yoo, D. J. Irvine, D. E. Discher and S. Mitragotri, *Nature Reviews Drug Discovery*, 2011, **10**, 521.